Flight Demonstration of Novel Atmospheric Satellite Concept

NIAC Phase II Final Report

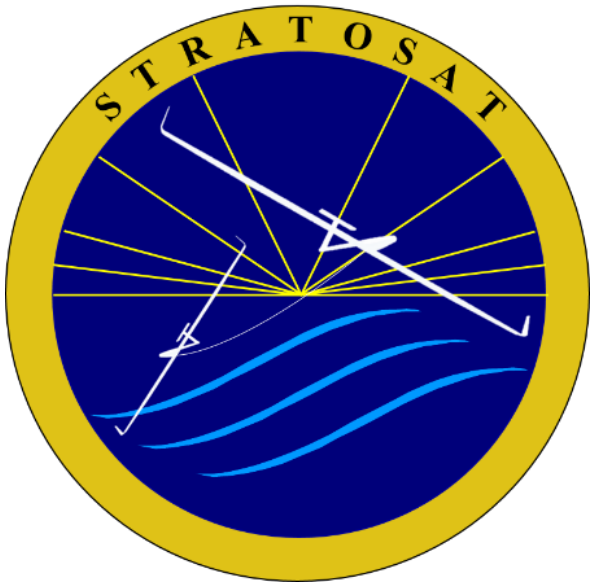

W. A. Engblom, PI
Embry-Riddle Aeronautical University

ERAU team contributors:
H. Moncayo (co-PI), N. Coulter (controls/avionics lead), T. Stone (mech systems lead), J. Willems and J. Lown (aero leads), E. Jacobs (pilot)

Additional contributors:
R. Decker (NASA MSFC), J. Wurts (consultant)

November 14, 2018

Executive Summary

The major focus of the Phase II effort described herein is to develop and demonstrate an aircraft capable of autonomously sailing (i.e., to cruise without propulsion or external assistance), and thereby prove that the dual-aircraft platform (DAP) atmospheric satellite concept is potentially viable. This sailing mode of flight was identified as the #1 enabling technology required for the stratospheric DAP concept (also known as *Stratosat*) in the NIAC Phase I effort. No scientific demonstration of this technology has ever been done or documented to our knowledge. This report describes efforts to take a major step towards the sailing mode of flight capability using a single aircraft connected by cable to a moving ground vehicle which uses sufficient crosswind to cruise without propulsion while "pulling" the ground vehicle forward (i.e., without external assistance).

The development of a prototype aircraft is described in terms of novel and key hardware and software elements. A specialized prototype aircraft is described, including a novel cable release mechanism, novel "lateron" control surfaces, and a highly-accurate onboard wind measurement system. Additionally, a novel means to safely connect the aircraft to the moving ground vehicle is described involving a fishing rod/reel and integrated load cell. All of these devices were designed and developed in house and validated in flight testing. Software is developed to provide look-up tables that give the flight condition targets (i.e., 3-D position relative to ground vehicle, forward speed, aircraft orientation, etc.), based on current wind speed and direction. These tables are successfully validated in flight simulation and used onboard the aircraft. High fidelity analysis of the aircraft aerodynamics are described – required to produce accurate target sailing flight conditions. A novel wind tunnel measurement technique is developed to accurately assess the aerodynamics of the ultra-thin cable.

A new specialized flight simulator is described which is utilized to develop and verify the flight software required onboard the aircraft, and to support training of pilots for flying the aircraft while tethered to a ground vehicle. The DAP flight simulator was developed within the Matlab-Simulink framework and included detailed treatment of aircraft/cable aerodynamics, cable dynamics, experimentally-derived propeller-motor thrust curves, actuator responsiveness, and realistic air turbulence. The specialized formation flight controller algorithm, developed using this flight simulator, and onboard the aircraft is described. Finally, a novel auto-tuning software is described and verified within the flight simulator that is shown to refine the sailing flight condition targets during flight using an optimization technique involving doublet maneuvers. Virtual flights using the auto-tuning software indicate that the prototype aircraft should be able to reach and hold sailing conditions despite moderate levels of turbulence provided there is sufficient mean wind available.

An overview of the flight testing program is provided. Hundreds of short flights were conducted, primarily using a "dead" short runway at Deland Municipal Airport which permitted use of a moving ground vehicle. Additional flight tests at Space Florida's Shuttle Landing Facility are also described. First year results from these tests in which the aircraft is controlled manually, demonstrated that excessive flight testing would be required for a pilot to learn to sail with visual cues. However, second year results from autonomous flight these tests included successful demonstration of the closed-loop autonomous formation flight capability (i.e., autonomously determine, reach, and hold the required 3-D location relative to the ground vehicle required for sailing). The next step of using the auto-tune software to autonomously refine the aircraft orientation targets to finally achieve sailing remains the primary goal of future work.

Table of Contents

1.0 Introduction

1.1 Background

Airborne platforms which could stationkeep in the stratosphere for years, sometimes referred to as *atmospheric satellites*, represent a long-standing, grand challenge to the aeronautics community, and have enormous potential societal and economic impact. Such platforms would diversify and expand surveillance capabilities (e.g., for NASA's earth science missions) and communications bandwidth and availability (e.g., for underserved remote areas), at a fraction of the cost of orbital satellite networks. Constellations of such platforms might potentially be integrated into the National Airspace System (NAS) to facilitate inter-aircraft communications, navigation or surveillance, or similarly for vessels along major shipping lanes. An atmospheric satellite may also facilitate extraterrestrial planet science missions.

NASA's Pathfinder and DARPA's Vulture programs, and more recently industry, has funded development of aircraft which rely on solely solar power for propulsion, as shown in Figure 1. These vehicles must accumulate and store a substantial amount of power during the day to operate at night. This is further compounded by the large variability of available solar energy during the year and the inability to point aircraft wings towards the sun to improve solar power capture. These factors result in severe limitations on the power that can be made available to the payload for communications, surveillance, etc.

Figure 1. Stratospheric solar aircraft development efforts (top: AeroVironment's Helios, Boeing's SolarEagle; bottom: Google's Solara, Airbus' Zephyr, Facebook's Aquila)

1.2 Dual-Aircraft Platform Concept

The Dual-Aircraft Platform (DAP), illustrated in Figures 2, is a patented concept for achieving a low-cost atmospheric satellite [1,2] which utilizes wind shear as the primary energy source, and has the potential to stationkeep for years at a time, while providing substantial levels of power for its payload. DAP consists of two glider-like Unmanned Aerial Vehicles (UAVs) connected via a thin, ultra-strong cable which literally sails without propulsion, using levels of wind shear commonly found in lower Stratosphere (e.g., near 60,000-ft). The two aircraft are positioned at different altitudes, as far as 2,000-ft apart, to encounter substantially different horizontal wind velocities (i.e., wind speed and/or direction). The device operates similar in principle to a kite-surfer (see corner image) in which the upper aircraft, referred to as the *SAIL*, provides lift for both aircraft and aerodynamic thrust, while the lower aircraft, known as the *BOARD*, primarily provides an upwind force to keep the platform from drifting downwind (also like the keel on a sailboat). In fact, all sailing vehicles use two separate (but connected) aerodynamic/hydrodynamic surfaces, both experiencing a different local flow velocity, to produce thrust.

The DAP aircraft derive power from solar cells, like a conventional solar aircraft, but also could extract wind power using the propeller as a turbo-generator when there is an excess of wind shear propulsion. Electric power is needed for the flight computer/controls, adjust the cable length, to use the propeller to produce thrust when needed, and for the onboard payload.

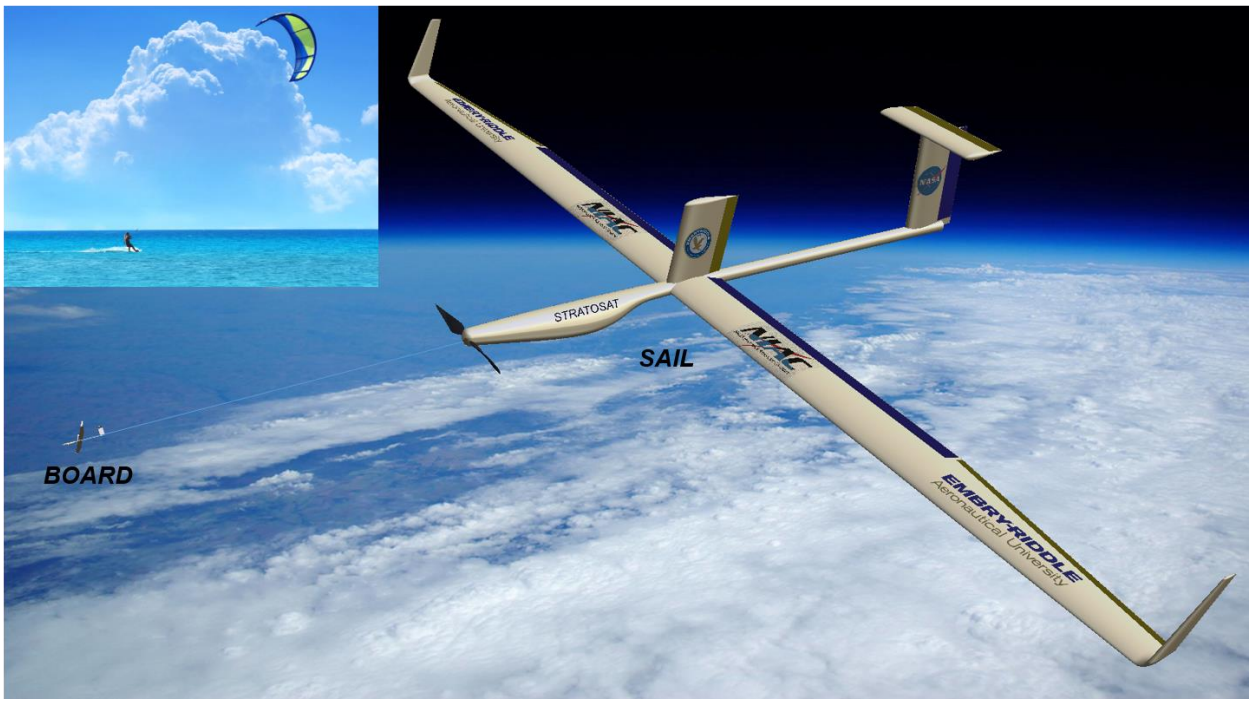

Figure 2. Dual-aircraft platform in sailing formation (kite surfer shown in upper left corner)

The theoretical basis of the DAP sailing concept is described in detail in the literature [1]. The guidance algorithm uses the atmospheric wind profile to determine the required aircraft altitudes, platform's ground speed and heading, aircraft orientations, cable tension, and lateral (horizontal) spacing using a constrained non-linear optimization problem. Provided stringent but realizable targets for aerodynamic and structural performance are met, it has been shown

theoretically that the device could achieve sailing conditions without propulsion roughly 99% of the time within 60,000-70,000 ft. This probability is attributed to the highly-persistent atmospheric circulation patterns, as depicted in Figure 3. The three recirculation cells (Hadley, Ferrel, and Polar) and jet streams (stream tubes) meander and change strength, but are persistent features which promote consistently strong vertical wind shear (i.e., changes in horizontal wind speed with altitude) in the lower Stratosphere, just above the tropopause (i.e., typically >50,000 feet).

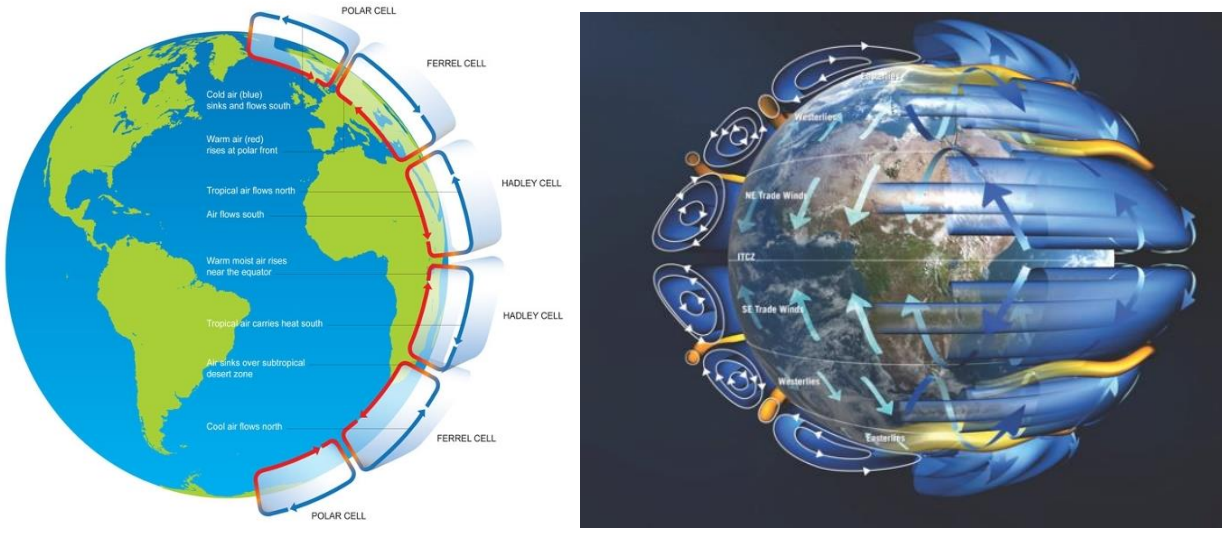

Figure 3. Earth's atmospheric circulation patterns just below the Stratosphere

1.3 NIAC Phase I Summary

The NIAC Phase I effort focused on evaluating the performance of a conceptual DAP design (see Figure 4) as a communications platform over central Florida. More specifically, this effort involved flight simulations of the DAP platform for month-long missions using realistic, synthetic wind environments derived from NASA KSC's 50 MHz Doppler Radar Wind Profiler. Details behind the flight simulation model, DAP configuration, wind environment, and GN&C software are provided in [3] and the NIAC Phase I Final Report [4].

The simulation results showed the DAP concept appears to be a potentially viable alternative to the pure solar aircraft as an atmospheric satellite, including as a localized communications relay. Flight dynamics simulation using a detailed transient atmospheric model show that, with accurate LiDAR forecasting of wind profiles, the platform could remain in sailing mode for the vast majority (> 90%) of a long duration mission, greatly reducing the need for propulsion, compared to a pure solar aircraft. Additionally, the flight simulation results show that the SAIL and BOARD aircraft collects significantly more solar energy than the pure solar aircraft. The latter is related to the advantageous use of solar cells/film on both the upper and lower surfaces of the aircraft wings.

The Phase I effort also identified the most critical and challenging technological advancements (i.e., a technology roadmap) required to enable the DAP concept to be realized. The reader is referred to [4] for the related discussion. The Phase I effort identified the need to develop/demonstrate the novel DAP sailing mode of flight (i.e., using wind shear without propulsion) as the most crucial enabling technology hurdle.

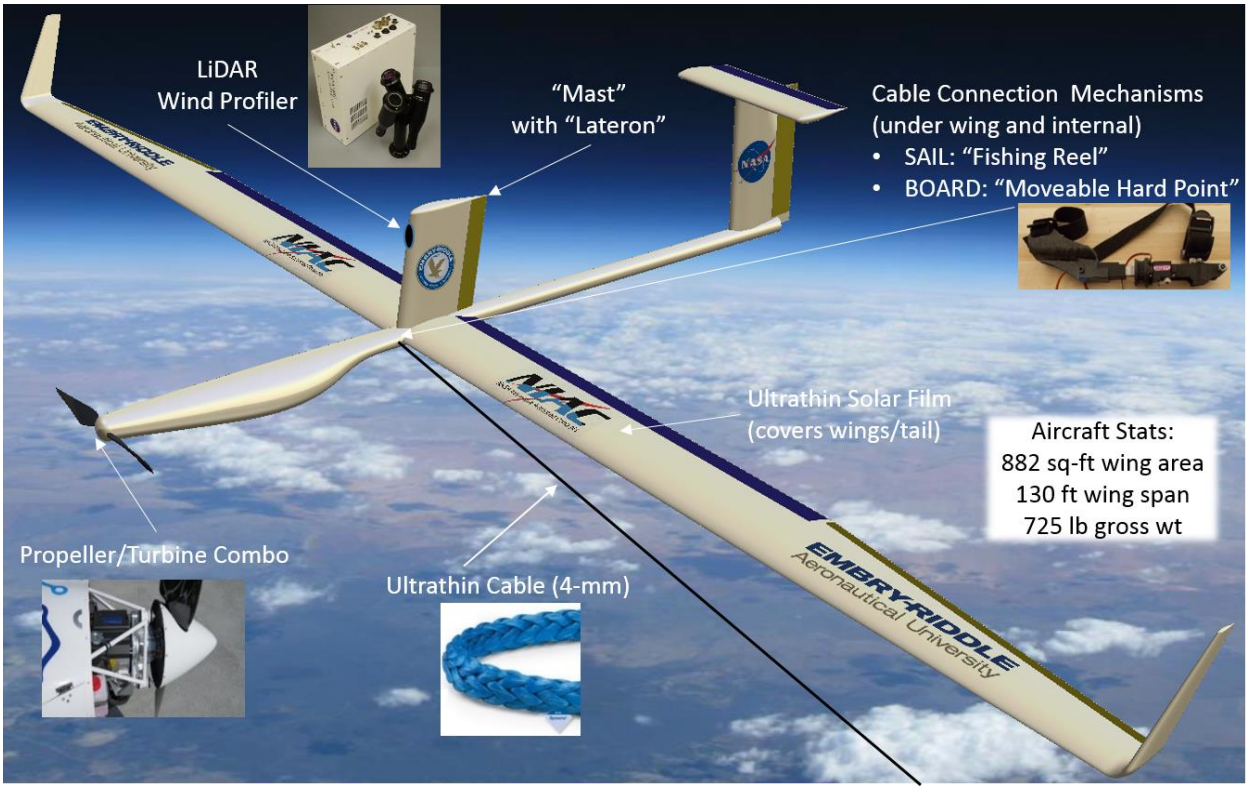

Figure 4. DAP conceptual design developed during NIAC Phase I

1.4 Phase II Objectives

The primary objective of the Phase II effort was to conduct the first scientific flight demonstrations of the DAP sailing mode of flight (i.e., cruise without propulsion using wind shear) at Space Florida's Shuttle Landing Facility (SLF) using vertical wind shear below a 400 feet ceiling. Theoretically, sailing mode is attainable provided the aircraft is sufficiently aerodynamically efficient (i.e., high lift-to-drag (L/D) ratio), structurally efficient (i.e., low weight-to-wing surface area (W/S)), and there is sufficient vertical shear.

Figure 5 illustrates the location of the SLF, including the baseline take-off and landing zones along the runway. The proximity of Weather Tower 313 is advantageous in terms of permitting real-time monitoring of winds aloft since a moderate strong cross-wind, relative to the runway, is necessary to achieve the sailing mode of flight.

This primary objective implies the crucial related objectives of developing/validating a novel special-purpose, glider-like aircraft (i.e., something like a subscale version of the Figure 4 prototype), including novel:

- Efficient, composite airframe with "lateron" control surface(s)
- Cable related mechanisms
- Avionics package
- Special-purpose GN&C flight software

A new DAP flight simulator, with hardware-in-the-loop capability, was also deemed a crucial development item, necessary to support pilot training and autonomous flight control software development. Development and testing of flight test procedures for use at the SLF, and obtaining related FAA approval, is another important objective relative to safety. Each of these aforementioned related objectives are discussed subsequent chapters.

Figure 5. Space Florida's Shuttle Landing Facility and nearby Tower 313

Preliminary flight testing was conducted involving two remotely-controlled (R/C) Timber aircraft connected by a nylon cable (see Fig. 6) to evaluate the potential to achieve the sailing mode with solely manual (pilot) operation. Two experienced, certified R/C pilots each operated one of the two aircraft while connected, in calm wind conditions. Despite using headsets to communicate, the pilots found difficulty to produce and hold a level of tension in the cable.

Figure 6. Two R/C Timbers connected by a nylon cable while attempting to hold line tension

Based on the aforementioned preliminary flight tests, it was decided to reduce the complexity/risk of the Phase II study by focusing on operating ONE aircraft connected by a thin cable to a moving truck (not another aircraft). An example of this scenario is depicted in Figure 6 below. By operating within a crosswind, relative to the moving truck's path, the aircraft is theoretically capable of sailing (i.e., cruising without use of propulsion), while "pulling" the truck forward (i.e., without assistance from the truck). Note that the targeted 3-D position, of the glider relative to the truck, depends on the wind conditions, and the lateral spacing shown is only representative of these tests. The glider is also always positioned ahead of the truck, relative to the truck's path.

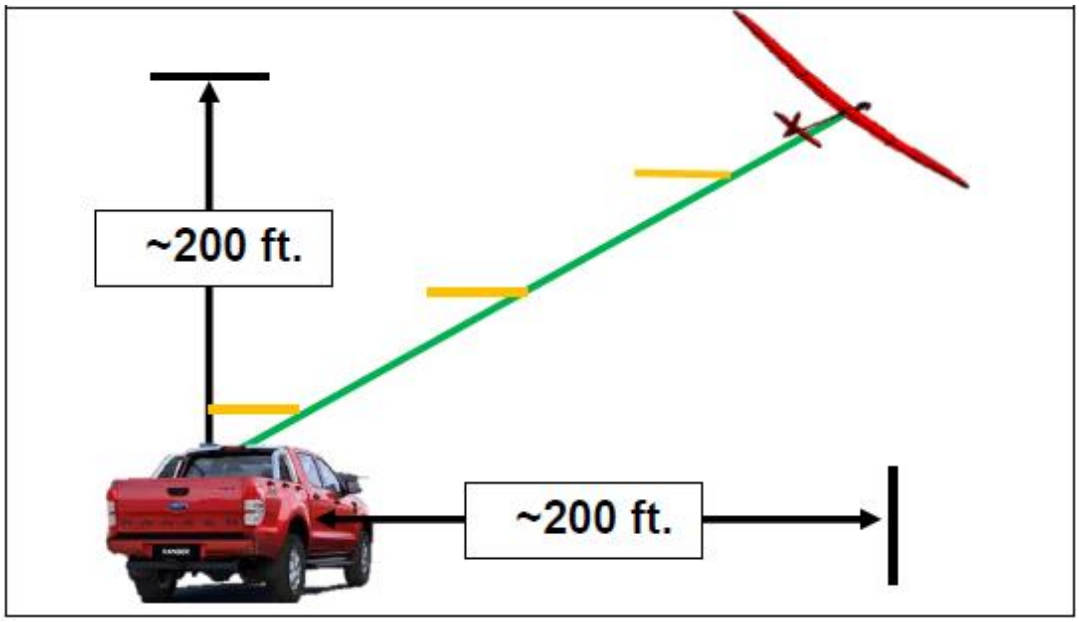

Figure 6. Glider connected to moving truck via cable (green) with streamers (yellow); Glider's position target relative to truck depends on wind conditions

2.0 Prototype Aircraft

2.1 MAXA Pro Airframe

The well-known MAXA Pro4M carbon-fiber/Kevlar composite airframe was selected as the basis for the small fleet of prototype aircraft used in this study. This 4-m wingspan aircraft weighs less than 3-kg (~6 lb) fully-loaded (i.e., including all avionics, battery, motor etc.). This airframe is widely used in glider competitions internationally, offering the exceptional aerodynamic and structural efficiency required for the DAP prototype. Figure 7 shows "T1" (for test aircraft #1) and Table 1 includes specifications for the aircraft and cables used in flight tests.

Figure 7. DAP aircraft configuration

SPECIFICATIONS	Aircraft (SAIL)
Wing Planform Area	8.8 ft² (0.82 m²)
Total Mass	6.0 lb (2.75 kg)
Wing Span	13.1 ft (4 m)
Aspect Ratio	19
Airfoil Section	Proprietary
Wind Speed Limit	~20 knots
CABLE	
Material	Nylon/Dyneema®
Cable Length	280 – 500 ft
Cable Diameter	0.70 mm/0.35 mm
Rated Strength	50 lb

Table 1. Aircraft/cable specifications

2.2 Lateron Development

Novel control surfaces that we call "laterons" were originally identified during Phase I work to be highly advantageous for aircraft control during the sailing mode of flight. This was confirmed with the new DAP flight simulator to be discussed later. These surfaces work to provide a pure lateral force and permit a novel control strategy, also to be discussed later.

Two lateron systems were designed, built the composites lab, and tested. Lateron Prototype 1 (LP1) is an all-moveable, centrally-mounted "dorsal fin" (also called "mast" in Phase I effort) that lies atop the center of the main wing (see Fig. 8). LP2 is a set of twin all-moveable vertical fins (or laterons) which are mounted at the junctions between the center and outer wing-tip sections (see Fig. 9). LP2, unlike LP1, doesn't contaminant the airflow reaching the tail, and can sit closer to the wing structure. The total surface planform area is roughly identical for both LP1 and LP2, resulting in similar expected control authority. Each are built using fiberglass and Titanium materials.

LP2 was selected and implemented on aircraft "T3" and "T4", and used in all flight testing during the second year of the Phase II effort. Note that LP1 could be added to the prototype to effectively double the total lateron planform area.

Figure 8. Lateron Prototype 1 (LP1) – centrally located "Mast" (wing tips removed)

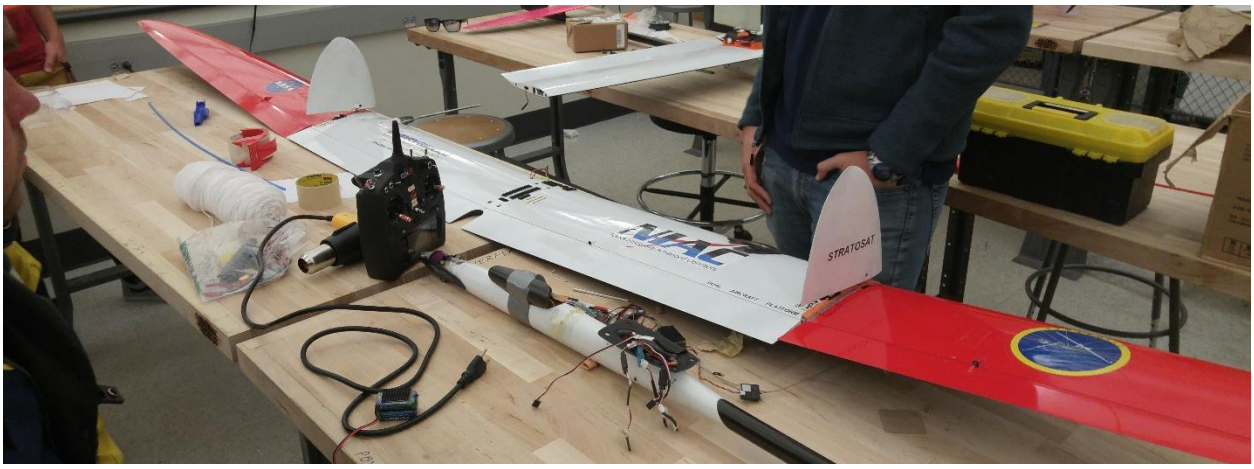

Figure 9. Lateron Prototype 2 (LP2) – twin "fins" at each wing section junction (fuselage detached)

2.3 Cable Connection System

Figure 10 includes images of the various cable connection mechanisms that were developed for use onboard the aircraft. These mechanisms are 3-D printed and then permanently embedded (internally) within the fuselage below the main wing. This location is to minimize the unwanted torque imposed on the aircraft due to cable tension forces in flight.

These designs permit for rapid release of the cable from the aircraft via a servo-driven pin actuator. Once the pin in actuated, the white collet (see left figure) falls thru a slot from the aircraft, carrying the connected cable. The final versions of the mechanism include a curved pin release rather than inline pin release. A 0.7-mm diameter nylon monofilament cable (50-lbf test) was selected for flight testing.

Figure 10. Cable connection/release mechanism with servo-driven linear pin (left); Subsequent versions of the cable release mechanism shown without servos/pins (right)

Early-on in the Phase II study, the team developed an alternative cable connection mechanism that allows for both external attachment to the fuselage and greater flexibility of the placement of the connection along the fuselage. As indicated in Fig. 11, the mechanism is connected via two straps along the underside of the fuselage. The cable connected point is moveable due to use of a linear actuator which slides up to 4 inches. Based mainly on the reliable operation of the internally connected mechanisms in flight tests, the team decided not to utilize this externally-connected mechanism in flight tests.

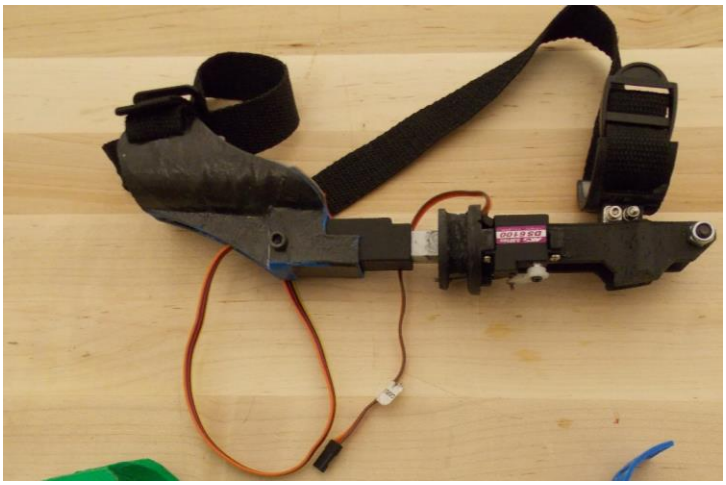

Figure 11. Externally-mounted, linear-actuated cable connection/release mechanism

2.4 Additional Structural Components

Manufacturing techniques such as 3-D printing and casting and curing of composite parts was crucial to the effort. Beside the major components of laterons and cable connection mechanisms, the team had to develop several smaller parts using in-house manufacturing. Figure 12 includes images of the light-weight motor mounts, and related tools (left), avionics shelf with stiffeners (center), and ring stiffeners for fuselage (right) that were manufactured for integration with the prototype airframes.

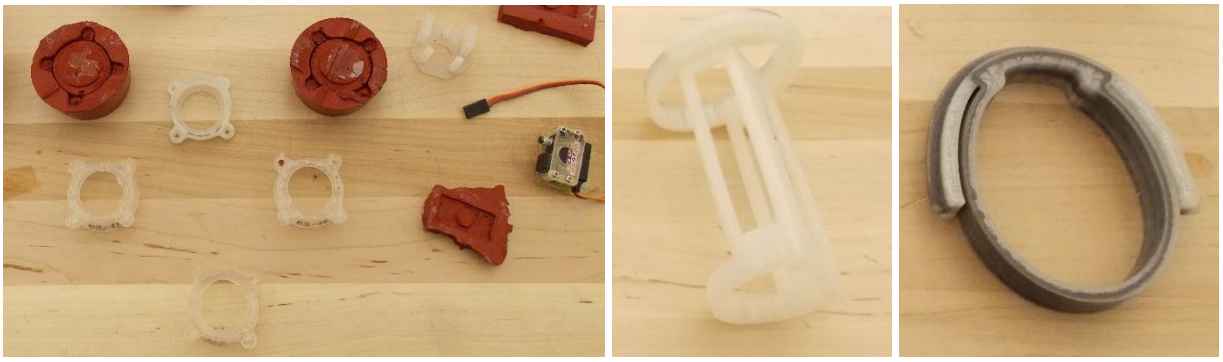

Figure 12. Motor mount and tools (left); avionics shelf (center); ring stiffener (right)

2.5 "MANTA" Airframe

Although not utilized in the Phase II study, an effort was made to design and build tooling for layups of a new carbon-fiber airframe center-section, called MANTA, which is expected to improve the aerodynamic performance and maintainability of the prototype. This center could substitute for the current MAXA Pro4M glider center-section and still be compatible with the original MAXA wing tips and tail structure. In Figure 13, MANTA is the gray portion of airframe in image on left below, while the blue wing tips and tail are from original MAXA. The main idea is to house the growing number of required avionics components within an enlarged "blended" fuselage to reduce the drag penalties associated with attaching these items outside the fuselage, and to reduce the weight of this relatively heavy portion of the airframe. Thus, this new airframe is expected to significantly improve the potential of the aircraft to sail, especially when attempting to fly two connected aircraft. However, the team decided to halt development of the required tooling and focus on continued use of the MAXA airframe.

Figure 13. MANTA center-section in gray with MAXA wing tips/tail (left); manufacturing of tool for MANTA (right)

2.6 Fishing Rod/Reel Mechanism

A crucial element of the flight test equipment is what the team refers to as the "fishing reel mechanism." The cable that is attached to the aircraft at one end must also be attached to the moving truck. Instead of a rigid connection to the truck, the team chose to devise a novel fishing pool/reel mechanism (see Figure 14). A Futek load cell was mounted so as to get accurate transient readings of the line tension, which is an important indicator to evaluate the performance of the aircraft while attempting to sail. The ability to adjust the cable length during the flight testing is critical since the cable length target to achieve the sailing mode changes depending on the wind conditions.

Figure 14. "Fishing Reel Mechanism" with Futek load cell (left); Fishing pole/line in use during flight test in which pilot controls aircraft (right)

This device is also very important from a safety perspective. The student holding the fishing pole can adjust the length of the line during ascent (i.e., let the aircraft pull out the line), and avoid undue line slack which poses safety concerns, including potential to entangle the pilot. Figure 14 (right) shows the fishing reel mechanism in use while the pilot is controlling the aircraft. Finally, in the event that the cable release mechanism fails, the student may cut the line to free the aircraft for a safer landing.

2.7 Avionics Configuration

The avionics includes all off-the-shelf components. The onboard flight computer and sensors were integrated within the airplane with the hardware architecture as shown in Figure 15. The primary on-board flight computer (OBC) used on DAP is a PixHawk v2 (PX4). PX4 is a commercial platform that features an ARM Cortex M4 processor with a principal clock of 168MHz. This processor runs the Nuttx real-time operative system which contains drivers for on-board sensors such as accelerometers, gyroscopes, barometer, magnetometer and GPS. In addition, the OBC has a microSD slot for data logging, ADC, a DSM interface for RC receiver antenna, and communication buses such as UART, SPI, CAN and I2C, and a 2MB flash for data logging.

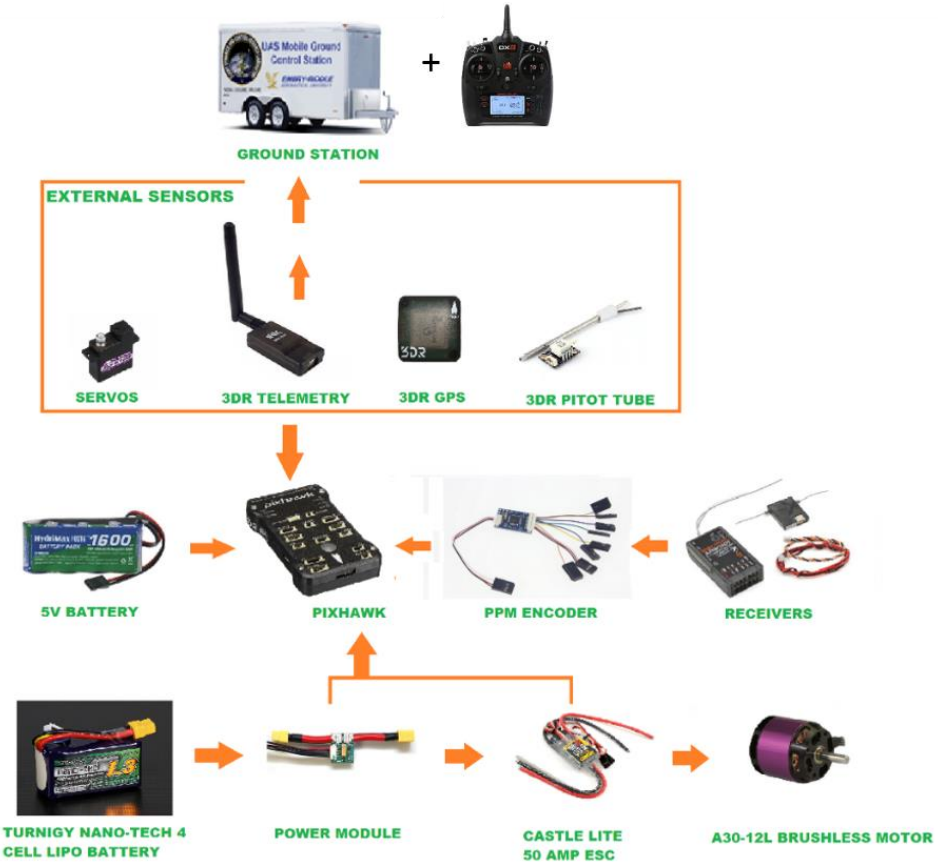

Figure. 15 Avionics Hardware Architecture

The environment used to program the OBC is the Mathworks® Pixhawk Pilot Support Package (PSP). This PSP generates ANSI/ISO C from Simulink® models explicitly created for Pixhawk flight management unit. Additionally, the PSP was enhanced at the ERAU's Flight Dynamics and Control Research Lab (FDCRL) with additional drivers to facilitate DAP missions. This interface allows for the customization algorithms that leverage onboard sensor data and supplementary calculations at runtime.

A number of sensors are interfaced with the flight computer for measuring and estimating different flight parameters including vehicle position, angular rates, accelerations, velocity. The sensor suit includes a uBlox LEA-6H high performance GPS, a PX4 digital airspeed, a ST Micro L3GD20H 16-bit gyroscope, a ST Micro LSM303D 14-bit accelerometer / magnetometer, an Invensense MPU 6000 3-axis accelerometer/gyroscope, MEAS MS5611 barometer. Additionally, OBC runs an Extended Kalman Filter with sensor bias corrections to estimate flight states such as vehicle attitude.

Reliable communications between the ground and the aircraft is vital for flight safety. An 8-channel transmitter is by the pilot for remote control and to switch to and from autopilot control. A 9-channel receiver for carbon fuselages with two satellites is utilized for reliable communication. When the aircraft loses communication with the ground, the autopilot initiates a fail-safe program in which the aircraft does a slow, spiral landing.

2.8 Air Data System

The aircraft has both a conventional 1-hole pitot probe (mounted on right wing junction) and an in-house designed/built/tested 7-hole air data probe (mounted on left wing junction), as shown in Figure 16. The 7-hole probe is used to obtain accurate readings of relative wind speed and direction, which can be used to determine the local wind speed and direction using other measurements and a Kalman filter. Knowledge of the wind speed and direction is critical towards defining the target flight conditions to achieve a sailing flight mode.

Figure 16. Prototype aircraft with pitot probe and 7-hole air data probe on opposite wings (left); 7-hole probe and pressure transducers (center) and front view of 7-hole probe (right)

3.0 Flight Simulator/Trainer

A realistic flight simulator is a crucial asset for developing the autopilot software that would be needed onboard the aircraft to autonomously achieve the sailing flight mode. Also, this simulator was considered necessary to train the pilots to position the aircraft in a sailing flight condition. Consequently, significant effort was made to increase the fidelity of the simulation capability, where possible, including high-fidelity analysis of the aerodynamics of the aircraft and cable.

3.1 DAP Simulation Environment Overview

The simulation environment developed and used for this Phase II investigation is shown in Figure 17. A modular structure within MATLAB/Simulink is adopted for portability, flexibility and extension capability for new aircraft models, autonomous flight algorithms, and guidance law development and testing. Simulink also has the capability to be interfaced with X-plane 10 for visualization of DAP performance. The simulation environment utilized for the virtual demonstration of the SLF flight includes vehicle models (for *SAIL* aircraft and *BOARD* truck), cable dynamics model, wind model, X-plane 10 simulation interfaces, a pilot-in-the-loop interface or autonomous flight controller, and provides statistics regarding DAP performance. More documentation on this simulator development may be found in [5, 6].

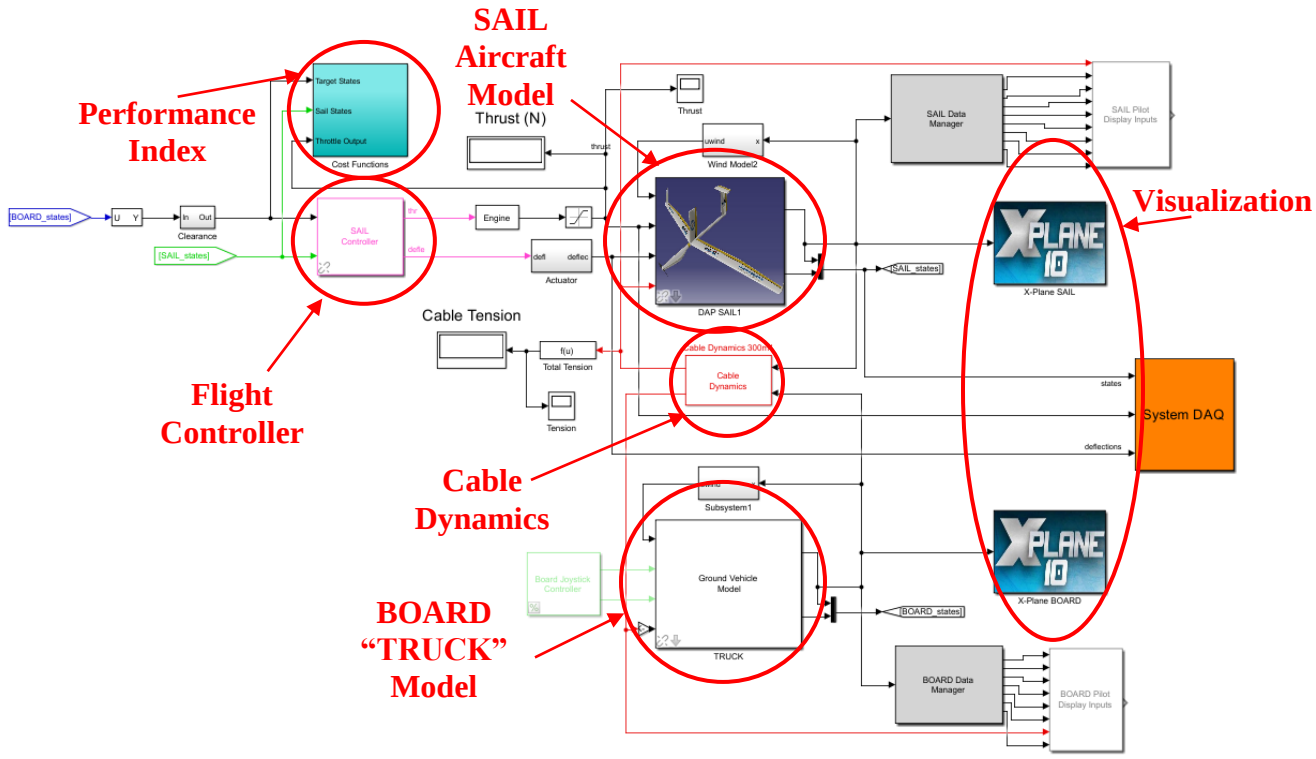

Figure 17. Simulation Environment of the Dual-Aircraft Platform

3.2 SAIL Aircraft/Truck Models

An Aircraft Library, known as Airlib, was utilized as the baseline configuration for the aircraft (referred to here as the "*SAIL*") model in the simulation environment. The library consists of aircraft models for use in Simulink based off of the FDC Toolbox. Airlib contains several general aircraft library blocks each including the six degree-of-freedom (6-DOF) aircraft equations of motion [7]. The blocks have the ability to operate in both continuous-time or discrete time with nonlinear general aircraft models. Using Airlib, the type of aircraft represented by the general aircraft dynamics block can be specified by the inertial and aerodynamic parameters sent to the model.

The *SAIL*'s aircraft model contains the aerodynamics model, the system's forces and moments model, and the aircraft's 6-DOF calculations. The generalized UAS model utilized in the simulation environment is shown in Figure 18. The aerodynamics model consists of look-up tables for the aerodynamic coefficients with respect to the aircraft's angle of attack (α), sideslip angle (β), and control surface deflections for the MAXA Pro 4m Glider. An accurate aircraft aerodynamics model is crucial for this proof-of-concept research program, and is discussed in the next section.

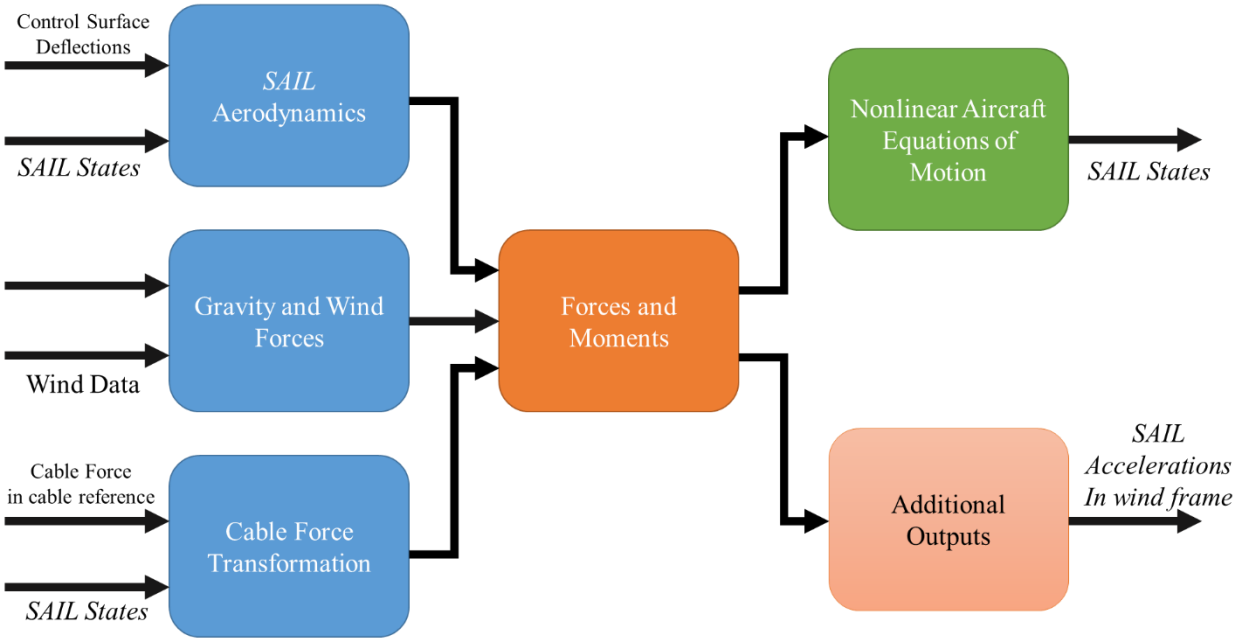

Figure 18. MAXA Pro 4m Glider model diagram.

The truck model (referred to here as the "*BOARD"*) is merely a vehicle moving at a prescribed fixed speed and heading along the runway. Consequently, there is no flight controller applied to this vehicle. The *SAIL* aircraft "pulls" the truck forward via cable tension, but the SAIL's force on the truck is so small that it can be neglected. This truck may be replaced with a second aircraft, but the Phase II effort focuses on the aircraft-truck combination only.

3.3 Detailed Aircraft Aerodynamics Evaluation

An accurate evaluation of the aerodynamics (i.e., estimation all relevant static and dynamic coefficients) is vital to the success of this effort. Our consultant completed an industry-like aerodynamics assessment using a Vortex Lattice Method (VLM) approach which also includes viscous flow effects from XFOIL. Specifically, the static aerodynamics coefficients have been tabulated versus angle-of-attack, sideslip, and for all control surface deflections (i.e., elevator, rudder, ailerons, flaps). Dynamic aerodynamics coefficients have also been provided in a tabular form. These tables are currently used in DAP flight simulations.

A high-fidelity Ansys-Fluent computational fluid dynamics (CFD) model has also been developed which utilizes a relatively new transitional Reynolds-Averaged Navier Stokes (RANS) flow model to accurately evaluate the laminar-to-turbulent transition effects on the MAXA Pro. This method was validated against experimental data (e.g., see Figure 19) for different airfoils and then applied to the full 3-D MAXA Pro aircraft. This CFD model was used to evaluate the aerodynamics for a matrix of cases involving all control surface deflections. Direct comparison with the VLM-XFOIL method shows adequate agreement except at higher angles-of-attack at which the higher-fidelity CFD model capture tip stall effects (see Figure 20), resulting in restricting use of the aero model to angles-of-attack of 6° or less. A detailed description of the DAP aerodynamic evaluation is found in [8].

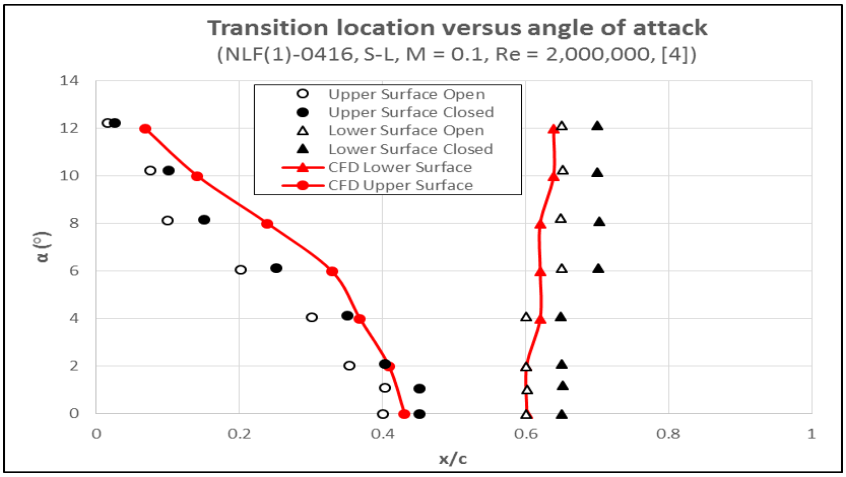

Figure 19: Transition location vs angle of attack for CFD and Experiment (for NLF airfoil)

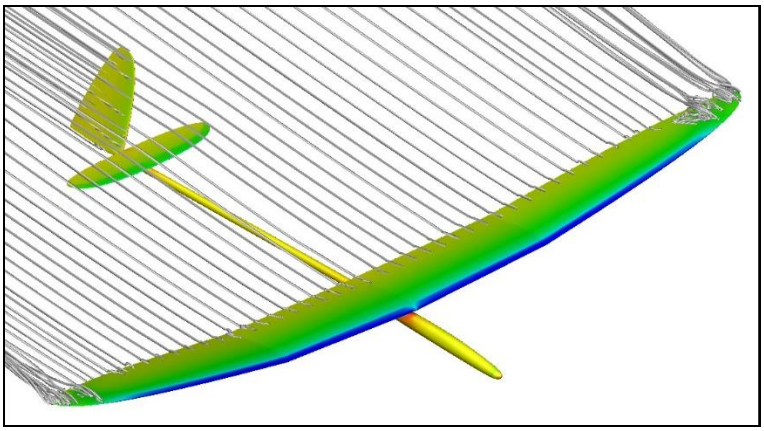

Figure 20: Full glider solution with streamlines and pressure contour at α = 8º

3.4 Cable Aerodynamics Evaluation

The accuracy of the flight simulator (and sailing tables to be discussed later) is limited by the accuracy of software inputs like cable drag coefficient. In order to improve the accuracy of the cable drag predictions, a novel wind tunnel test approach was adopted in which cable material is used to hang a steel ball within the wind tunnel test section (see Figure 21, left). The resulting cable curvature can be used to determine the cable drag coefficient with very good accuracy because the drag of a sphere is well-characterized as a function of Reynolds number. One important finding was that the braided, 0.35-mm diameter 50# test Dyneema cable originally selected for the Phase II study produces a significantly higher drag coefficient than a smooth, 0.70-mm 50# test nylon monofilament cable material, and nearly as much drag force. Nylon was subsequently selected for all remaining flight testing considering this small drag penalty and that pilots prefer elasticity of the nylon. The normal force coefficient of 1.30 for the nylon cable was adopted for all flight simulations.

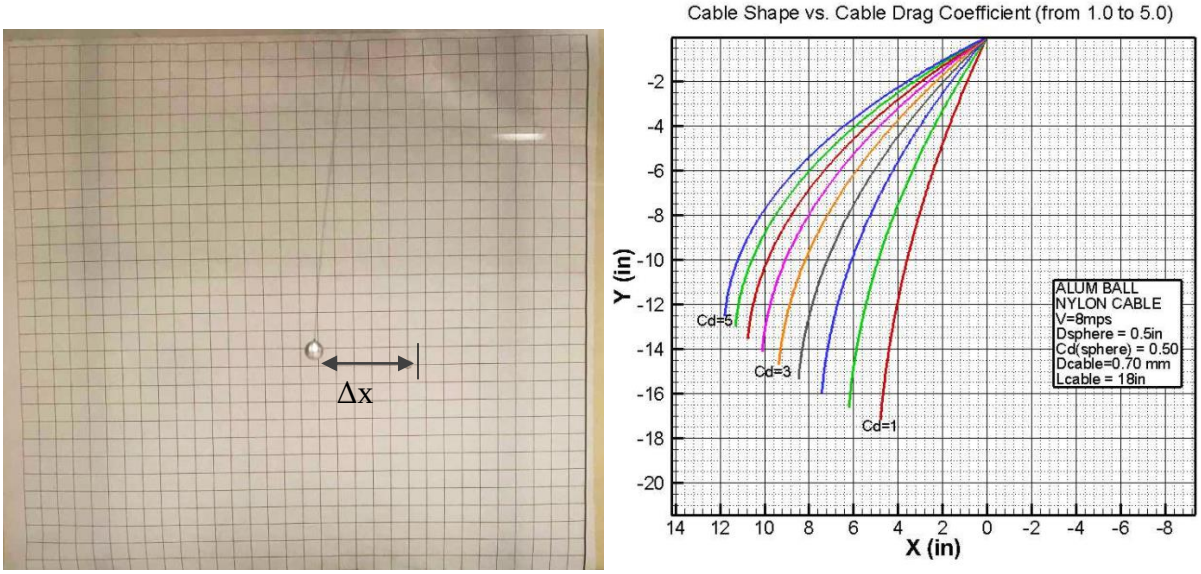

Figure 21. Steel ball/cable in wind tunnel (left); Analytical cable shapes from which to determine the best fit drag coefficient (right)

3.5 Lateron Model Development

The sailing mode of flight imposes a challenging controls problem for the DAP system. The target flight conditions consist of: aircraft ground speed and heading (same as ground vehicle), aircraft three-dimensional spacing relative to the ground vehicle (i.e., altitude, forward, and lateral spacing), and aircraft attitude (i.e., roll, pitch and yaw angle). As a result of reaching the target conditions, the cable attains a specific level of line tension. The attitude and spacing requirements result in a highly coupled system. Ideally these coupled requirements should be

uncoupled to allow the glider prototype to more easily attain and hold sailing conditions, as discussed below.

The glider prototype includes a novel, additional control surface on the main wing known as the *lateron*. At first, the lateron was modeled as a single fixed "mast" with a control surface much like a vertical stabilizer and rudder configuration, as shown in Figure 2. However, the final lateron configuration utilized on the actual aircraft, previously referred to as "LP2", involves two half-sized all-moveable control surfaces located along each wing (see Figure 22). Note that the laterons are centered over the vehicle's center of mass to generate nearly a pure side force. The lateron aerodynamic effects on the vertical stabilizer/rudder are neglected in the aerodynamic modelling. This side force generator decouples the dynamics involved for sailing flight for the lateral spacing and the roll angle requirements. With the employment of the lateron, the ailerons are now more easily able to maintain the aircraft's desired roll angle while the lateron maintains the lateral spacing between the *SAIL* and *BOARD*, as will be discussed later.

CFD analysis using Ansys-Fluent was conducted on the new configuration to generate look-up tables for the static aerodynamic coefficients versus aircraft angle of attack and sideslip. The transitional RANS approach described previously for the aircraft aerodynamics were applied to a single full 3-D lateron model, isolated from the aircraft.

Figure 22. Prototype aircraft with double lateron configuration (surfaces identified by white circles).

3.6 Flap Model Approach

The pitch angle and desired altitude are also coupled when using a conventional aircraft control surface configuration. Based on flight simulation, the elevators were deemed inadequate to maintain both the desired pitch and desired altitude when the aircraft attempts to achieve the sailing mode of flight [6]. In order to decouple the vertical spacing and pitch angle requirements, the flaps are used to maintain the altitude (i.e., vertical spacing between the two vehicles). To generate both a positive and negative pitching moment, the flaps are capable of positive and negative deflections, limited to 10° in upward deflection and 60° in downward deflection. This allows the flaps to maintain the required sailing flight vertical spacing and enabling the elevators to maintain the desired pitch angle.

3.7 Actuator Models

All of the actuator models used in the DAP simulation environment employ a first order transfer function to simulate the servo mechanical dynamics of the prototype. Since the flight controller can command an instantaneous change in desired control surface deflection, the transfer function limits the rate of change of the deflections for each respective control surface to

reflect the limitations of the servos. The transfer function limits the rate of change to 60°/0.2s corresponding to the glider's servo actuation speed. The first order transfer function to limit the actuation response is defined as:

$$G(s) = \frac{5}{s+5}$$

With a cutoff frequency of 5 Hz, the transfer function limits the control response of the actuators to realistic response times acquired by the servo's manufacture.

3.8 Cable Dynamics Model

The DAP sailing concept hinges on the ability for an aircraft to maintain tethered flight with another vehicle. Therefore, the dynamics of the cable must be modeled to ensure a realistic simulation environment is created. The cable is modeled as a series of cylindrical cable segments of equal length with diameter (0.7-mm), density (1180 kg/m^3), cable stiffness (3.0 GPa) and ultimate tensile strength (0.5 GPa), to appropriately represent the nylon cables used in flight testing. The Nylon cable is rated for 222 N (50 lbf). Hence, a multi-DOF model of the cable dynamics enabling accurate simulation performance for the interaction between the connected vehicles.

As described earlier, the aerodynamics forces on the cable are also a crucial element for simulation accuracy. Also, the cable drag is a significant limiting factor on the ability of the aircraft to attain the sailing mode of flight. The aerodynamic forces of the cable are modeled utilizing Hoerner's approach to a "cylinder in crossflow" in which tangential and normal components are applied independently, and applied to each longitudinal segment of the cable. The normal force coefficient was derived from wind tunnel experimentation, as described earlier, and found to be ~1.30 for the 0.7-mm diameter Nylon monofilament.

3.9 Propulsion Model

The motor chosen for the MAXA Pro 4m glider was the A30-12L Brushless electric motor. To simulate the throttle response and thrust output, a motor model was developed to handle the forces and moments generated by this brushless motor. The model accepts the commanded throttle response from the autonomous flight controller and transforms that throttle response to a thrust output of the engine. From flight data and wind tunnel testing, a look-up table was developed for use in the simulation environment. This look-up table utilizes the commanded throttle response provided by the controller output as a percentage of throttle and the true air speed from the air data sensor. This provides an accurate thrust output based on wind tunnel measurements of the propeller performance at same conditions.

The wind tunnel testing positioned a Hacker A30-12L Brushless motor into the oncoming freestream airflow. The motor throttle was increased from 5% to 100% for three airspeeds which include 8 m/s, 10 m/s, and 12 m/s, which cover the range of expected speeds for sailing flight conditions. The airspeed was measured using a pitot-static probe and digital pressure indicators. For each airspeed, the throttle was advanced in increments of 5% to achieve the motor thrust performance curve. This performance curve is shown in Figure 23 for thrust output and correspond throttle setting for each airspeed tested.

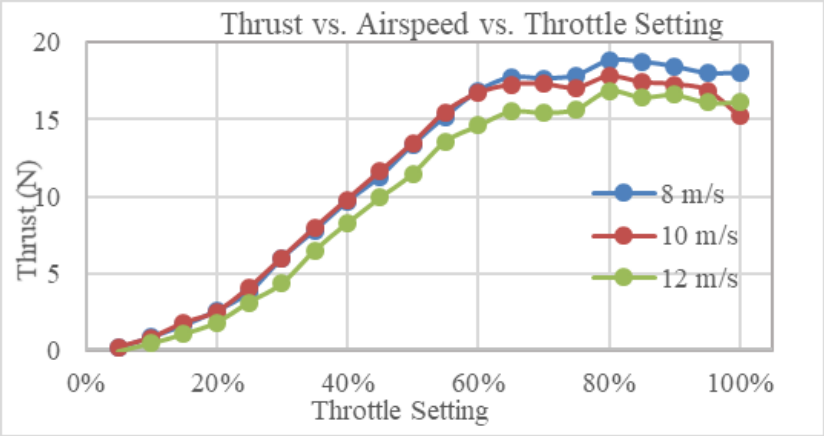

Figure 23. Thrust curve for DAP glider motor with respect to throttle setting and airspeed.

Since the flight controller can command an instantaneous change in desired throttle, an infinite impulse response (IIR) low pass filter with a time delay is used to limit the thrust response of the motor itself and to more accurately reflect the signal delay between hardware in flight. The IIR filter follows the discrete state space z-transformation form:

$$G(z) = \frac{1-e^{-aT}}{1-e^{-aT}z^{-1}} \quad \text{for } 10 * a * T < \pi$$

where a is the natural frequency of the system and T is the time step interval.

This IIR filter utilizes the discrete state space to design the transfer function, *G(z)*, to limit the throttle response to a commanded thrust rate output of 40 N/s. The latter was determined as an acceptable rate of change based on flight test data. This thrust output is then used by vehicle model of the *SAIL* aircraft.

3.10 Wind and Turbulence Model

The DAP concept relies on the wind shear between two tethered aircraft to maintain sailing flight conditions. Thus, to create an accurate simulation environment, a realistic, turbulent wind model needs to be implemented. The mean wind and turbulence models implemented into the DAP simulation environment are modeled using the Dryden wind turbulence model. This mathematical representation is widely used for aircraft design and simulation. The turbulence intensity level can be selected by the user to represent the strength of the turbulence and the resulting variations in the wind velocities. For DAP simulation testing purposes, six levels of turbulence severity are used to characterize the possible wind conditions that may be encountered in flight. Table 2 shows the turbulence levels with their corresponding standard deviations (STD) in both the wind velocity components and magnitude. In general, turbulence severity levels between 0-5 are considered low turbulence conditions; turbulent severity levels between 5 and 10 are considered medium turbulence intensities; and turbulence severity levels above 10 are considered highly turbulent conditions. The mean wind speed and direction magnitudes are also parameters that the user can initialize before running the simulation. These inputs are set in the simulation within the "Wind and Turbulence Model" section of the Matlab-Simulink model described in section 3.1.

Table 1. Turbulence Intensity Characterization

Turbulence Severity	Turbulence Intensity [%]	Mean SAIL Velocity [m/s]	STD of Turbulence Magnitude [m/s]	STD of Turbulence Component Velocities [m/s]		
				u	v	w
1	0.39	10.00	0.0388	0.0348	0.0619	0.0391
2	0.78	10.05	0.0776	0.0698	0.1238	0.0781
5	1.94	10.17	0.1938	0.1759	0.3102	0.1946
10	3.88	10.40	0.3881	0.3573	0.6240	0.3881
15	5.84	10.65	0.5841	0.5447	0.9428	0.5823
20	7.83	10.90	0.7825	0.7384	1.267	0.7765

3.11 Look-up Table of Sailing Mode Flight Conditions

The target flight conditions for sailing (i.e., aircraft cruise at steady speed and altitude without propulsion) are a critical component for the flight simulator. An optimization-based FORTRAN routine, previously described in the Phase I Final Report [4] for stratospheric flight, was adapted to generate target flight conditions for sailing for the SLF aircraft-truck scenario. This routine is simplified to replace the lower *BOARD* aircraft with a ground vehicle moving at constant speed and heading. This change effectively reduces the number of constraints imposed on the routine. The code is used to generate a table of target sailing mode flight conditions to cover the range of all possible wind speeds and directions to be experienced at the SLF. This table is read into the flight simulator and used to interpolate appropriate sailing mode flight conditions during the simulation.

Table 3. Excerpt from sailing mode flight look-up table for SLF along 330° heading

WIND (m/s)	DIR (deg)	ALTS (m)	VGR (m/s)	FWD (m)	RIGHT (m)	PSI (deg)	THE (deg)	PHI (deg)	LEN (m)
3.09	20	30.49	8.89	3.05	-47.6	-20.3	4.27	-30.8	54.5
3.09	24	30.49	9.07	3.26	-43.9	-19.6	4.34	-29.7	51.4
3.09	28	30.49	9.29	3.27	-40.1	-18.9	4.39	-28.4	48.4
5.14	24	30.49	7.67	7.59	-35.6	-10.8	4.15	-26.7	45.4
5.14	28	30.49	7.81	8.36	-35.4	-9.6	4.24	-26.7	45.4
5.14	32	30.49	7.98	9.08	-35.2	-8.6	4.33	-26.7	45.4

Table 3 provides an excerpt of one of the tables used for DAP simulation for which the runway is oriented like the Shuttle Landing Facility along 330° path from due North. The look-up tables provide the necessary data for the formation flight control to achieve sailing flight. They organize the data with respect to wind direction and wind speed. The aircraft must maintain the specific flight configuration to enable sailing mode flight. The parameters in the look-up table for sailing flight are organized as the wind speed (WIND) and direction (DIR), *SAIL* aircraft altitude (ALTS), ground speed (VGR), horizontal spacing relative to the *BOARD* (ground vehicle) in the forward (FWD) and right (RIGHT) directions, the yaw (PSI), pitch (THE), and

roll (PHI) Euler angles and the targeted stretched cable length (LEN). All of these parameters must be maintained to fly in sailing mode.

3.12 Architecture of Control Laws

DAP utilizes a formation flight controller with a separate inner and outer loop control architecture [6]. The general two-aircraft (*SAIL-BOARD*) tracking problem is defined based on the formation geometry center. The required sailing flight attitude and spacing requirements are generated previous to each flight based on the current wind conditions. The formation flight controller calculates the three-dimensional spacing in relation to a desired virtual point. The outer control loop minimizes the distance and velocity errors corresponding to the desired point and the actual state of the aircraft while the inner loop generates the necessary throttle output and control surface deflections to reach the desired state. Figure 24 represents the general control framework with the formation controller, inner and outer loop control loops.

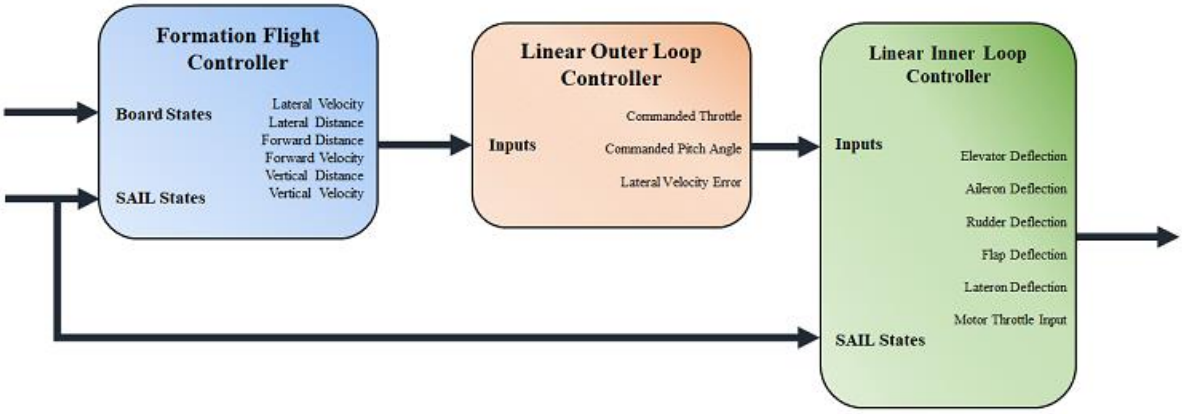

Figure 24. Block diagram of the Formation Flight control system for DAP simulator.

Formation Flight Controller

The formation flight control can be defined by two independent problems: a horizontal-plane tracking problem and a vertical-plane tracking problem. These tracking problems are analogous to a leader-wingman formation flight with the system utilizing the geometry based on the follower aircraft's reference frame and its location in an inertial space with respect to the leader aircraft [9]. The horizontal-plane and vertical spacing is predefined by the sailing flight requirements for the DAP system. These sailing flight requirements provide the horizontal and vertical spacing requirements that the *SAIL* must maintain to achieve sailing flight. The horizontal geometry is defined by a forward distance error, f, and a lateral distance, l. The vertical geometry is then defined by the vertical distance error, h.

For the horizontal spacing, the errors between desired position and actual position for the *SAIL* with respect to the *BOARD* can be calculated with the following relationships:

$$l = \frac{V_{By}(x_B - x) - V_{Bx}(y_B - y)}{V_{Bxy}} - l_c \tag{1}$$

$$f = \frac{V_{By}(y_B - y) + V_{Bx}(x_B - x)}{V_{Bxy}} - f_c \tag{2}$$

where l_c and f_c correspond to the desired lateral and forward clearance respectively. V_{Bn} corresponds to the velocity of the *BOARD* projected along axis *n*, n_B is the position of the *BOARD* and n refers to the position of the *SAIL* along the n^{th} axis. $V_{Bxy} = \sqrt{V_{Bx}^2 + V_{By}^2}$ is the velocity of the *BOARD* projected onto the $x - y$ plane. Taking these relationships for the lateral and forward distances, the *SAIL's* lateral and forward speed can be derived from the time derivatives of the lateral and forward distances respectively. The lateral and forward velocities are required for the formation control and are calculated as:

$$\dot{l} = \frac{V_{Bx}V_y - V_{By}V_x}{V_{Bxy}} + \Omega_B f \tag{3}$$

$$\dot{f} = V_{Bxy} - \frac{V_{Bx}V_x - V_{By}V_y}{V_{Bxy}} \pm \Omega_B l \tag{4}$$

where $\Omega_B = \frac{q_B \sin\phi_B + r_B \cos\phi_B}{\cos\phi_B}$, the trajectory-induced angular velocity in the $x - y$ plane around the vertical axis.

In flight, the positions and velocities of the *BOARD* and *SAIL* can be measured using the GPS on-board the ground vehicle and aircraft. Thus, the position and velocities from the formation flight geometry calculations can be orientated and projected along the *x* and *y* axes of the Earth-fixed reference frame. Eq. (5) represents the transformation matrix that will orientate the errors to a reference frame positioned along the *BOARD*'s velocity,

$$\begin{bmatrix} l \\ f \end{bmatrix} = \begin{bmatrix} \sin(\chi_B) & -\cos(\chi_B) \\ \cos(\chi_B) & \sin(\chi_B) \end{bmatrix} \begin{bmatrix} x_B - x \\ y_B - y \end{bmatrix} - \begin{bmatrix} l_c \\ f_c \end{bmatrix} \tag{5}$$

where χ_V is the azimuth angle. A trigonometric expression for the azimuth angle is given as:

$$\cos(\chi_B) = \frac{V_{Bx}}{\sqrt{V_{Bx}^2 + V_{By}^2}} \quad \text{and} \quad \sin(\chi_B) = \frac{V_{By}}{\sqrt{V_{Bx}^2 + V_{By}^2}}.$$

The vertical distance error, *h*, can be obtained using the vertical distance error relationship:

$$h = z_B - z - h_c \tag{6}$$

where the time derivative is given by:

$$\dot{h} = V_{zB} - V_z \tag{7}$$

Outer Controller

Following the formation flight controller, the outer loop controller has a similar configuration with two components, a 'vertical' controller and a 'horizontal' controller. The outer control loop is responsible for minimizing the distance and velocity errors provided by the

formation flight. The vertical, lateral and forward errors are compensated for by producing a commanded motor throttle response, bank angle, and pitch angle respectively. The following linear control laws provide the commanded response to minimize the distance and velocity errors:

$$\phi_d = K_{\dot{l}}\dot{l} + K_l l \tag{8}$$

$$\delta_T = K_{\dot{f}}\dot{f} + K_f f \tag{9}$$

$$\theta_d = K_{\dot{h}}\dot{h} + K_h h \tag{10}$$

In these differential equations, the proportional gains K_n are designed using conventional linear design methods.

Inner Controller

The inner loop controller is implemented to minimize undesirable disturbances in the system while providing the tracking capabilities required to track the target attitude and throttle response. A linear approach is implemented again for the inner controller to stabilize the system.

The vertical controller commands both the flaps to maintain a desired altitude while the elevators are used to maintain a desired pitch angle in flight. The flaps δ_f use the commanded pitch angle, θ_d, to generate a flap deflection to achieve the desired altitude. The elevator controller δ_e must track a predetermined pitch angle, θ_{sail}, based on the sailing conditions. This controller includes a stabilizing term based on the pitch rate, *q*, feedback and a roll compensating term based on the absolute value of vehicle's roll angle. Eq. (11) and (12) show the control laws designed for the vertical control system:

$$\delta_f = \left(K_{P\theta} + (1/s)K_{I_\theta} + sK_{D\theta}\right)(\theta_d - \theta) \tag{11}$$

$$\delta_e = \left(K_{P\theta} + (1/s)K_{I_\theta} + sK_{D\theta}\right)(\theta_{sail} - \theta) - K_{Pq}q + K_\phi|\phi| \tag{12}$$

The lateral controller generates an aileron δ_a, rudder δ_r, and lateron δ_l deflections. The aileron and rudder deflections are generated to track a predetermined sailing condition similar to the elevator controller. The roll and yaw angles, ϕ_{sail} and ψ_{sail} respectively, are specific to the aircraft's heading and the wind direction and speed to achieve sailing flight. However, the lateron deflection is generated to track the lateral velocity error from the outer loop. These controllers have stabilizing terms implementing the pitch and yaw rates, *p* and *r* respectively. Eq. (13) through (15) show the lateral control system:

$$\delta_a = \left(K_{P_{a_\phi}} + (1/s)K_{I_{a_\phi}} + sK_{D_{a_\phi}}\right)(\phi_{sail} - \phi) - k_{Pap}p - k_{Par}r \tag{13}$$

$$\delta_r = \left(K_{P_{r_\psi}} + (1/s)K_{I_{r_\psi}} + sK_{D_{r_\psi}}\right)(\psi_{sail} - \psi) - k_{Prp}p - k_{Prr}r \tag{14}$$

$$\delta_l = \left(K_{Pl_\phi} + (1/s)\mathrm{K}_{\mathrm{I}_{l_\phi}} + sK_{Dl_\phi}\right)(l) - k_{Plp}p - k_{Plr}r \quad (15)$$

Equations (11) to (15) show the relationship used to design the controllers responsible for commanding the desired control surface deflections where where δ_n is the control surface: flap, elevator, aileron, rudder and lateron. Proportional, integral, and derivative gains are denoted as K_{Pm}, K_{Im}, and K_{Dm} respectively. The Euler angles, θ, ϕ, ψ have subscript *d* and *sail* to indicate the desired formation state and sailing condition, respectively.

3.13 Visualization

The DAP simulation environment developed in Simulink has the capabilities to interface with the X-Plane 10 flight simulation environment. The X-Plane flight simulator communicates with the Simulink model and graphically displays the information from Simulink into real-world 3D space with *SAIL* and *BOARD* models created in Blender's 3D graphics software toolset. Virtual demonstration of sailing flight with both the *BOARD* (behaving as the ground vehicle) and the *SAIL* in the X-Plane 10 3D environment is depicted in Figure 25. Using an external plugin for X-Plane 10, X-Plane can communicate with a separate computer on the same network. This allows for the simultaneous real time communication between a computer that runs the simulation environment in Simulink and another computer or computers that runs the X-Plane program for visualization. Figure 26 shows setup in full use with two computers running X-Plane and one computer running the simulation. The Simulink model sends the states of the *SAIL* to one computer with X-Plane while the states of the *BOARD* are sent to second computer running X-Plane. This system allows for the full visualization of the DAP concept in a real world environment.

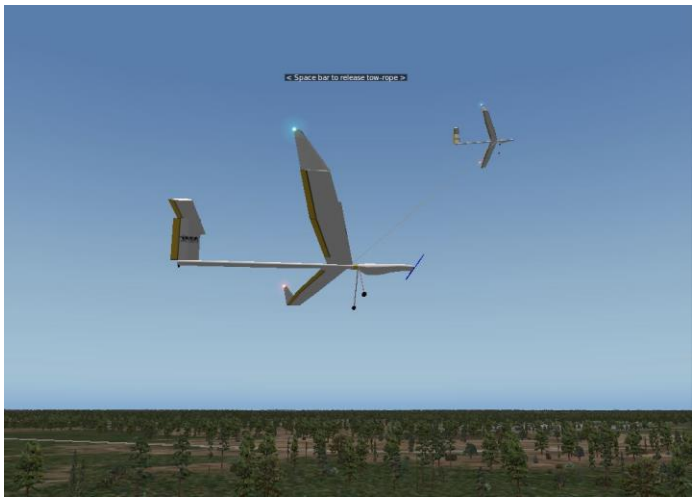

Figure 25. *SAIL* aircraft connected to *BOARD* aircraft, representing the ground vehicle, via a Nylon cable, as displayed with X-Plane

3.14 Simulation Pilot-in-the-Loop Capabilities

Utilizing the same visualization setup with X-Plane 10, a pilot can use the simulation environment as a flight training program. With a Radio Control (RC) transmitter connected to the host computer running the simulation, the X-Plane visuals can be set to create a similar

scenario representative to the real-world *SAIL* and truck tethered flight. This pilot-in-the-loop training allows the pilot to obtain visual cues and practice flying the UAS to target conditions before enabling the autonomous flight controller. This flight training is important because the entire mission can be simulated for the pilot to understand tethered flight dynamics for take-off, turbulent wind conditions, and landing scenarios before the glider prototype is flown. Another important aspect of the pilot training involves the pilot's ability to obtain an approximate 3D spacing with the required sailing conditions. The closer the pilot can bring the aircraft into its sailing flight orientation, the less control effort is required by the formation flight controller to obtain sailing conditions. This will reduce any oscillations the controller may cause when enabled with large initial distance and velocity errors from the sailing flight target spacing.

Figure 26. Pilot-in-the-loop HUD

4.0 Sailing Flight Optimization Algorithm

DAP sailing mode of flight requires that two tethered aircraft (or one aircraft connected to a ground vehicle in this research effort) to maintain aircraft altitude and speed without the need for propulsion. Two connected aircraft can only sail if sufficient wind differential exists (i.e., vertical wind shear) across the altitude range of the two aircraft. However, sailing flight conditions for a single aircraft connected to a ground vehicle only requires a sufficient crosswind velocity component since the ground vehicle is powered to maintain its own constant speed and direction.

A look-up table, similar in format to Table 3, was generated using the FORTRAN program briefly described in section 3.11. This table covers all possible wind speeds and directions (i.e., with sufficient crosswind component relative to the truck's path along the runway at the Shuttle Landing Facility). The tables provide a best initial guess for the flight conditions for sailing; however, the assumptions behind the calculations of this look-up table are not precise. For example, there will be onboard sensor error (e.g., measuring wind speed and direction) that creates uncertainty about the required target flight conditions for sailing. Furthermore, there is uncertainty regarding all the physical parameters and models used to compute these look-up tables. For example, the actual cable aerodynamic drag is not precisely known in part since the atmospheric wind profile along the cable is not measured during flight. Another level of flight optimization, referred to herein as *autotuning*, is needed to resolve on-the-fly the challenges presented by the inherent uncertainty in the pre-optimized flight conditions from the look-up tables.

4.1 Sweeping Angle Autotuning Method

The Sweeping Angle Autotuning Method (SAAM), described in [10], is capable of generating sailing flight conditions through a passive calculation strategy. The sailing optimization process requires a precalculated solution from the look-up table to initialize sailing flight. The aircraft first achieve and maintain the required lateral, vertical and forward position (or "clearance" relative to the truck) from the look-up tables, using the formation flight controller previously described in section 3.11.

SAAM then begins to optimize the current flight condition for sailing flight based on a performance index consisting of trajectory tracking, thrust monitoring, and control surface actuation cost functions to determine when a new sailing flight condition is achieved. Attitude doublets are performed autonomously to find the new aircraft attitude requirements to enable sailing flight mode. When performing these doublets, the performance index is capable of updating at a sufficient speed to capture the dynamics of sailing flight as the *SAIL* passes through the appropriate roll, pitch, and yaw angles. The performance index is used to identify new Euler angle targets, which are updated and sent to the formation flight controller. SAAM constantly looks to improve the attainment of sailing flight conditions (i.e., to overcome the uncertainties in the look-up tables) using the *SAIL*'s performance index and aircraft doublet maneuvers. A flow chart providing the process of SAAM to establish sailing flight conditions is provided in Figure 27.

SAAM does not guarantee that a sailing flight solution will be found since the limitations of this system depend on the accuracy and timely response of the performance index. Also, since doublet maneuvers must be performed, control logics must be implemented to ensure that the

doublets do not cause adverse effects on the aircraft's flight qualities when in tethered flight. Lastly, the response time of SAAM depends on how close the glider gets into sailing flight before initializing the doublet maneuvers. Therefore, SAAM's optimization power is directly linked to the accuracy of the look-up tables used to provide the initial conditions to start the angle sweeps. If there is a large discrepancy between the sailing targets and the data tables, SAAM may not be able to optimize the flight conditions and enable sailing flight. On the other hand, SAAM is expected to maintain sailing flight conditions even as wind conditions change, without having to reinitialize all targets using the look-up tables.

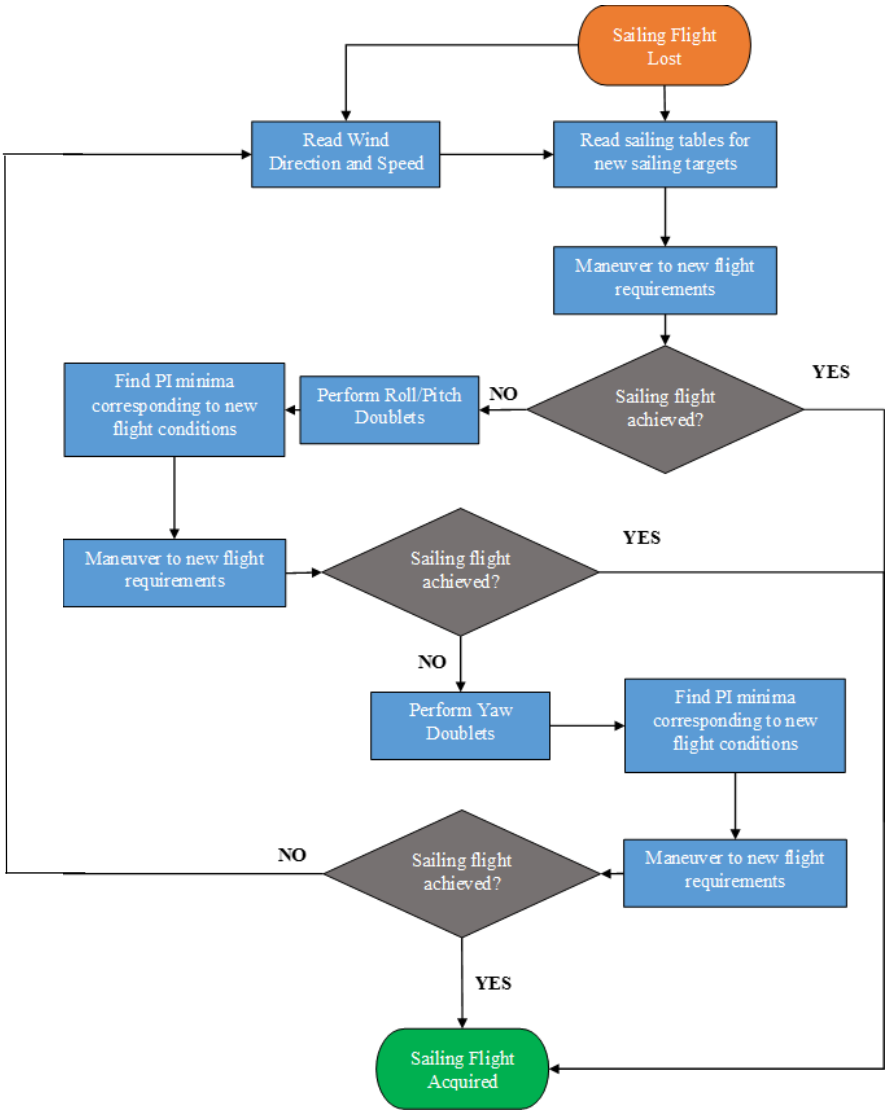

Figure 27. SAAM process flow chart for obtaining new sailing conditions.

4.2 SAAM Performance Index

To acquire quantitative measurements of the performance of the aircraft's current flight conditions, performance characteristics were defined to reflect sailing flight. Specifically, a performance metric was designed utilizing cost functions to track the errors in i) trajectory, ii) motor thrust activity, and iii) control surface deflections. Note that for sailing conditions to be achieved, the lateral, vertical, and forward spacing between the two DAP vehicles (in this case the aircraft and the ground vehicle) must be maintained to ensure cruise at constant velocity and altitude). Additionally, the motor thrust must be zero, and control surface deflections (i.e., flaps and laterons) ideally approach zero during sailing (and minimize aircraft drag). These three individual performance indices for the trajectory tracking, thrust, and control surface efforts are weighted to generate the combined performance index of the system (PI_{SAIL}):

$$PI_{SAIL} = \bar{w}_{TT} \cdot PV_{TT} + \bar{w}_{CA} \cdot PV_{CA} + \bar{w}_{T} \cdot PV_{T} \tag{16}$$

PV_{TT}, PV_{CA}, and PV_T are the individual performance indices for the trajectory tracking, control actuation, and thrust response, respectively. The derivation of each of these indices and validation exercises are documented in [10]. Preparation of a journal publication on this subject is currently underway. Each index is weighted using $\bar{w}_{TT}$, $\bar{w}_{CA}$, and $\bar{w}_{T}$, respectively, based on subjective and relative importance of each metric. For sailing flight, minimizing the thrust required to maintain the flight conditions is the most significant parameter for sailing. The weights used to generate the performance index responses in this study are summarized in Table 3.

Table 4. Performance Index global weights

Performance Weight	Value
$\bar{w}_{TT}$	0.15
$\bar{w}_{CA}$	0.15
$\bar{w}_{T}$	0.70

4.3 Autotuning Validation

Several test cases are defined and simulated, using the DAP flight simulation environment described in Chapter 3, to evaluate the capability of SAAM to attain and hold a sailing flight mode under different flight uncertainties. These uncertainties include i) wind measurement uncertainties, ii) sailing condition calculation errors, and iii) *SAIL* aircraft and cable aerodynamic uncertainties. Each case simulates an aircraft connected to moving vehicle moving along the runway heading of 330° (at Shuttle Landing Facility) while experiencing a pure crosswind of 60°, wind speed of 3.08 m/s (6 knots), and a moderate turbulence severity level of 5.

The sailing mode requirements, indicated by the sailing table discussed in section 3.11, include that the motor thrust remain zero while the *SAIL* maintains altitude (40.39 m), speed

(9.49 m/s), and heading (330°), and the cable connecting the two vehicles must remain under tension. If any of these three conditions is violated, the glider is no longer flying in sailing mode.

The first test case initiated the simulation with the *SAIL* outside of sailing mode with the initial conditions outlined in Table 5. The system was allowed to stabilize and achieve a steady state flight condition and then the autotuning algorithm was engaged. SAAM was able to optimize the flight conditions, shown in Table 6, to achieve sailing flight. This results shows that the autotuning method is capable of finding a new sailing mode. There are subtle differences in the aerodynamic forces assumed to create the sailing tables, and those computed in the flight simulator that results in a modestly different final aircraft orientation to achieve sailing. It is important to note that this aerodynamic uncertainty will occur in real flight as well.

Table 2. Initial conditions of *SAIL* (not sailing)

Parameter	Value
North Spacing	-23.75 m
East Spacing	-51.89 m
Vertical Spacing	47.87 m
Yaw angle, ψ	-9.79°
Pitch angle, θ	7.00°
Roll angle, φ	-15.00°

Table 3. Final conditions of *SAIL* (in sailing mode)

Parameter	Value
North Spacing	-23.75 m
East Spacing	-51.89 m
Vertical Spacing	47.87 m
Yaw angle, ψ	-13.79°
Pitch angle, θ	5.95°
Roll angle, φ	-21.62°

Figure 28 shows the performance index in the first 20 seconds of flight before the SAAM algorithm is applied. Off nominal sailing conditions (i.e., non-zero performance index) are indicated.

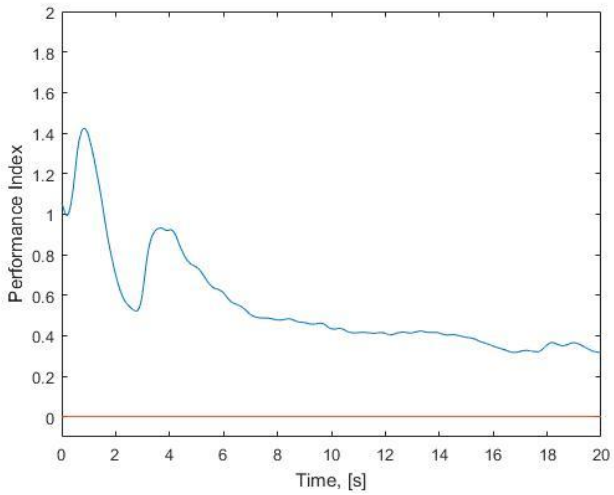

Figure 28. Performance Index during off nominal sailing conditions.

After 20 seconds, the SAAM algorithm is engaged and the *SAIL* begins the doublet maneuvers. The glider performs autonomous, coupled roll and pitch doublets in an attempt to sweep through varying attitude angles, and minimize the performance index. The new minimum of this performance index is then used to update the target attitudes (i.e., Euler angles).

Maintaining the newly optimized roll and pitch angles for the new flight condition, a yaw doublet is then performed to optimize the yaw angle of the *SAIL*. The formation flight controller now had an entirely new attitude to command. This new attitude enabled the UAS to achieve sailing flight around 120 seconds from the start of the simulation. This sailing flight is characterized by zero commanded thrust, a steady cable tension, and the performance metric goes to zero as the new flight conditions were held. Figure 29 summarizes the thrust output, cable tension, and performance index response for the entire SAAM process.

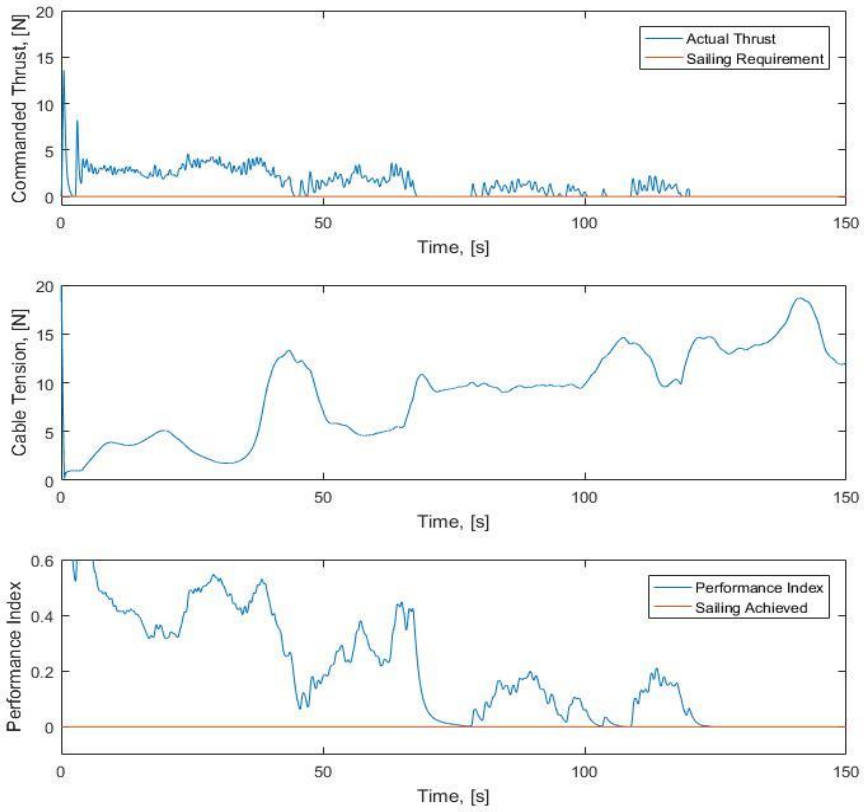

Figure 29. Thrust response, performance index, and cable tension for the entirety of the first SAAM test case

Additional test cases were designed and simulated to determine the capabilities of finding new sailing conditions given relatively large uncertainties in the wind conditions and aircraft/cable aerodynamics, as described in [10]. SAAM is shown to be very effective in re-optimizing the sailing flight conditions and enabling the *SAIL* aircraft to achieve "perfect" (i.e., performance index of zero) sailing flight conditions despite these significant uncertainties. Finally, the addition of moderate levels of wind turbulence are shown to cause the aircraft to infrequently need propulsion to re-attain sailing flight conditions, as expected. It is important to emphasize that these simulation results suggest that the prototype aircraft along with its novel flight guidance and control strategy can theoretically achieve the sailing mode, and real-world flight testing is an appropriate next step.

5.0 Flight Testing

Extensive flight testing was conducted during Phase II towards developing a system and operational procedure that could achieve the sailing mode of flight using a single aircraft connected via cable to a moving ground vehicle. As described below, three test sites were utilized. The Tomoka R/C field in Daytona Beach was used to conduct short solo aircraft flights. The Deland R/C field and its quarter-mile "dead" runway (alongside the Deland Municipal Airport) was used to conduct primarily formation flight testing, both without and with the cable attached. Space Florida's Shuttle Landing Facility (SLF) and its 5-mile long runway were used to conduct long duration flights involving autonomous formation flight and sailing.

The flight testing at Deland R/C field was approved by the Airport Manager and Deland R/C Club. This testing was crucial as it enabled the team to develop safe and reliable procedures for flights involving the aircraft connected to a moving ground vehicle. These procedures were the basis of the document provided to the FAA that eventually resulted in obtaining FAA-waiver for operations at the SLF.

5.1 Solo flight characterization at Tomoka R/C Field

During the Phase II effort, more than one hundred solo aircraft flights (i.e., without a cable attached) were conducted at Tomoka R/C Field in Daytona Beach using the four test aircraft (T1, T2, T3, and T4). The objectives of these solo flights included:

- **Shakedown**
  These flights evaluate motor/prop performance, control authority, avionics and telemetry performance. These tests were necessary each time hardware or software was changed on a test aircraft.
- **Fail-safe tests**
  These flights involve intentional evaluation of the onboard code to invoke and maintain autonomous flight when communication to the pilot is lost. The aircraft was programmed to fly in a slow spiral and eventually land. This capability was necessary to meet FAA requirements to eventually fly at the Shuttle Landing Facility.
- **Parameter identification**
  These tests involved the use of specific doublet maneuvers to provide data to predict aerodynamics coefficients in post-flight analysis for use in flight simulation. Results from these tests were not successful in producing accurate aerodynamics coefficients. Instead, high-fidelity numerical methods were used to determine the aerodynamics coefficients, as described in section 3.3.
- **Trajectory tests**
  These flights involve having the aircraft autonomously follow a preplanned trajectory as a preliminary step towards being able to autonomously maintain a specific clearance (i.e., 3-D position relative to a moving ground vehicle).

5.2 Attempts to Sail using Manual Remote Control (First year)

During the first year of the Phase II effort, the flight operations team focused on conducting flights at both Deland and the SLF in which the pilot attempts to manually, remotely control the aircraft into a sailing position and orientation. More specifically, the pilot attempts to position the aircraft into roughly the correct position relative to moving pickup truck (as specified by the sailing tables). The aircraft connected by cable to a student carrying the "fishing reel" mechanism described in section 2.6 which also measure line tension. Based on telemetry the pilot is instructed to move the aircraft into position while the truck is moving at a constant speed along the runway. Upon reaching this approximate position, the pilot attempts to orient the aircraft to extract energy from the wind and "pull" the truck, without propulsion. Although the sailing tables provide specific Euler angle targets, it was felt that the pilot should instead orient the aircraft based on visual cues and the current line tension, provided by another student watching tension data on a laptop.

Figure 30 shows the team preparing to start a flight test along the Shuttle runway. The pilot is standing while connected to the truck with a harness, while another student is holding the fishing pole/line that is connected to the aircraft, and another student is watching the line tension on a laptop while seated in the truck bed. Telemetry is read on a laptop held by a student in the passenger side of the truck cab (not visible) and is relayed to the driver and pilot, as needed.

Figure 30. Preparing to start flight test attempt to manually achieve sailing at the SLF

These early sailing attempts were not successful. Figure 32 provides a sample of data recorded during one of these sailing attempts. The altitude, throttle level, aircraft speed, and cable tension are shown. The pilot was able to hold an approximate 3-D position relative to the moving truck, maintain approximately the required ground speed, and was also able to sustain some tension in the nylon fishing line. However, the position, speed, and orientation of the aircraft has to be held more precisely, and the tension somewhat larger (e.g., 5 lb_f), to produce enough "thrust" to maintain cruise conditions without propulsion.

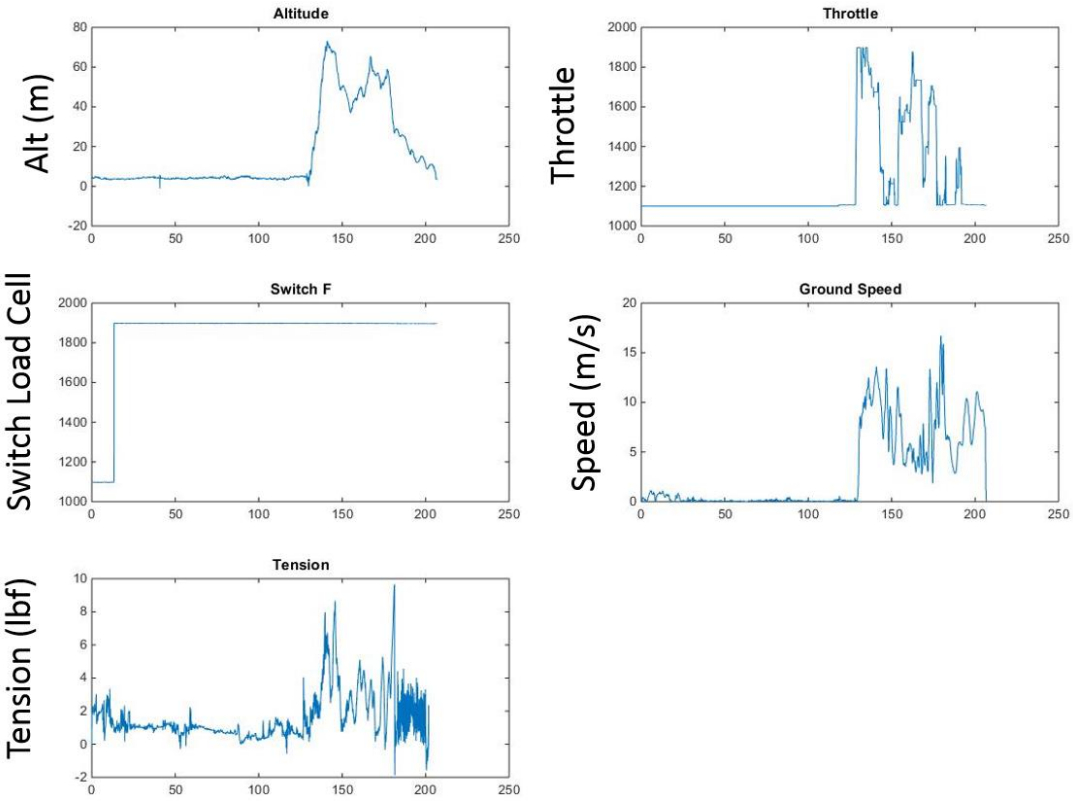

Figure 31. Telemetry and load cell data from a manual flight test


Figure 32. Manual control flight testing at Deland R/C field along runway from behind pilot (aircraft is connected via nylon line)

Figure 32 shows the flight test from a perspective close to that of the pilot during flight testing at the Deland R/C Field alongside Deland Municipal Airport. A major limitation of the manual approach is that the pilot can only respond to visual ques and sparse information provided to him. The pilot cannot "feel" the aircraft line tension like a kite surfer can. Although it may be possible for a pilot to learn to sail the aircraft, it would clearly be extremely difficult and take an excessive amount of flight testing to accomplish.

Figure 33 contains a team photo taken after flight testing at the SLF at the culmination of the first year of the Phase II effort. The two test aircraft, T3 and T4, used held by the ERAU DAP team. Despite the relatively long flights (i.e., > 10 minutes) enabled on the SLF runway, the pilot is unable to achieve sailing flight conditions. The team decided that a near full autonomous approach would be necessary to achieve the sailing mode of flight during the Phase II effort. Furthermore, the DAP concept would only be viable as a fully autonomous platform.

Figure 33. Flight testing at the Shuttle Landing Facility (test aircraft held by the ERAU team)

5.3 Formation Flight Development (second year)

During the second year of the Phase II effort, hundreds of flights were conducted at Deland R/C Field, on the "dead" runway alongside the active Deland Municipal Airport, to develop and tune the autonomous formation flight controller. Although the runway is only about a quarter-mile long, is provides a long enough distance to conduct formation flight tests in which a ground vehicle moves along the runway. Figure 34 provides a chase plane image of a flight test at the Deland R/C field. The truck is being driven along the runway with the pilot controlling the aircraft from a standing position behind the truck cab (while attached to truck along waist with harness). Another student controls the chase plane while seated.

Figure 34. Chase plane view of Deland airport flight testing of formation flight capability

Figure 35 demonstrates the quality of the autonomous formation flight controller. The time history of the target clearance (i.e., relative distance of aircraft from moving truck) for all three directions (i.e., lateral, forward, and vertical) is shown. The actual clearance clearly converges towards the target clearance within a short time period from take-off. This performance is sufficient to expect excellent performance along the much longer SLF runway in future flight tests.

The target clearance is determined by the aircraft autonomously. Specifically, the wind speed and direction is periodically measured by the air data system (see section 2.8) and then used to look-up the target sailing conditions using the onboard sailing tables (see section 3.11). Once the onboard computer chooses a target sailing condition, the aircraft moves towards the 3-D target clearance targets. If the winds are insufficient to enable sailing, the aircraft continues in level flight until wind conditions improve. Consequently, this type of flight test demonstrates a *closed-loop* autonomous formation flight capability.

The accuracy of the air data system was also validated during flight testing in Deland. Figure 36 demonstrates the capability of the air data system to adequately measure the wind speed and direction as compared to the wind conditions measured by the weather tower at the airport. The signal oscillations at the start and end of the flight are transients associated with take-off and landing.

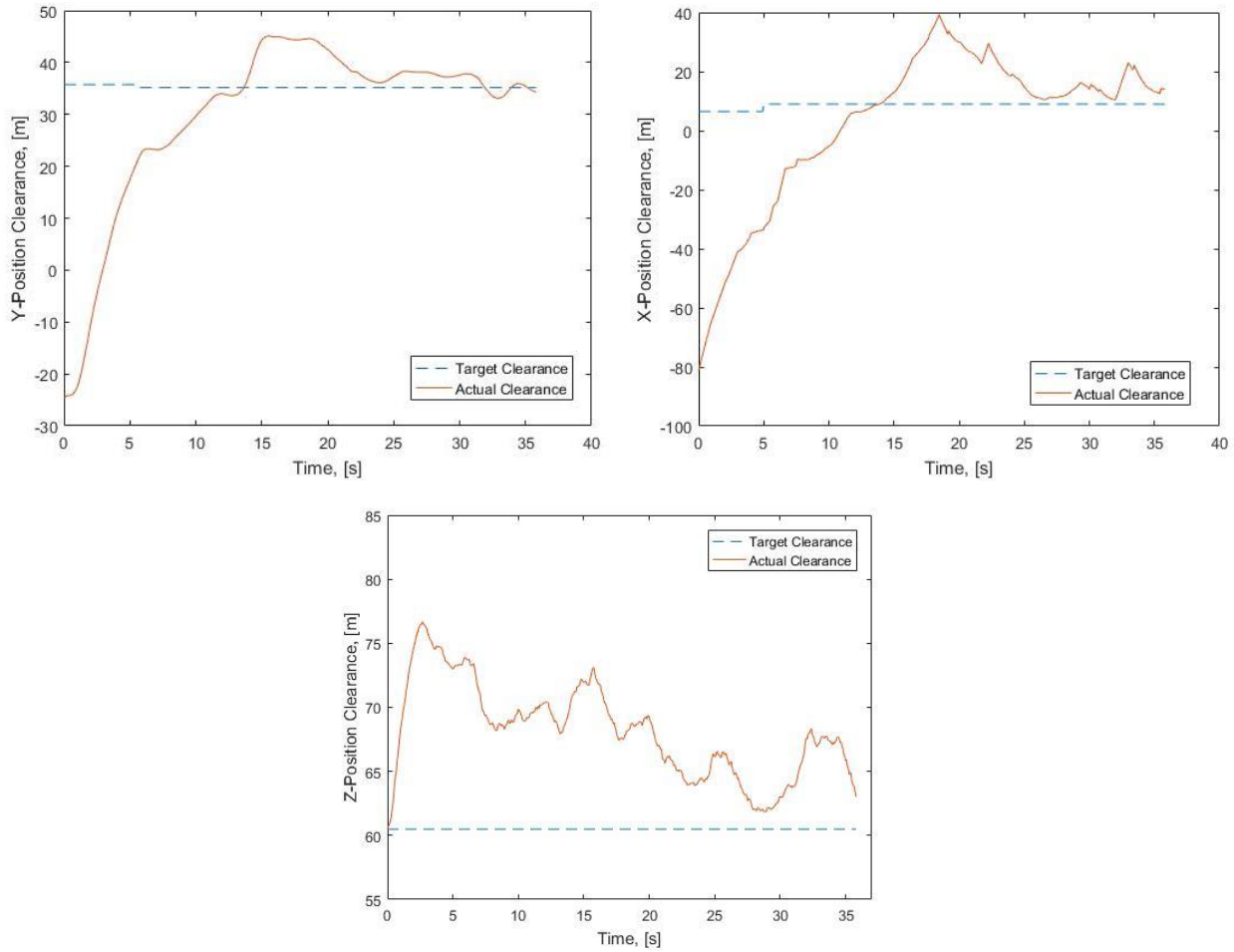

Figure 35. Formation flight clearance vs time for lateral (Y), forward (X), and vertical (Z) during Deland flight test along runway

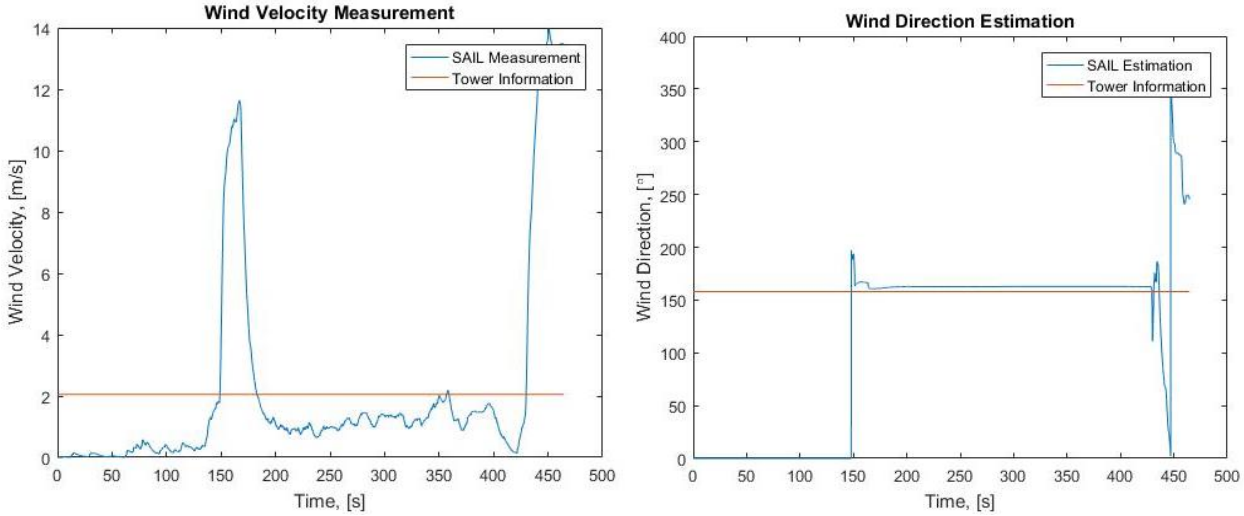

Figure 36. Air data system measured wind speed and direction during formation flight test at Deland compared with nearby weather tower information

5.4 Near-term Future Plans (post-Phase II)

The next, and crucial, development step is to have the aircraft, in addition to holding in formation flight, attempt to attain and adjust the target orientation (i.e., Euler angles) to achieve the sailing mode via the auto-tuning software described in Chapter 4. For these test, the aircraft must be connected to the ground vehicle via the nylon cable, using the fishing rod/reel mechanism, similar to the remote-controlled flight tests conducted during the first year of this effort. The cable tension is measured via the load cell integrated into the fishing rod, to confirm sufficient tension is held during post-flight analysis. Without the cable the aircraft would not be able to hold sailing flight conditions.

For these sailing flight attempts, the ground vehicle must approximately maintain the target ground speed and extended cable length, as determined from the onboard look-up (sailing) tables. These two values are periodically updated autonomously by the aircraft, and then transmitted to a laptop in the ground vehicle via telemetry. A passenger reads this data and directs the driver to attain and hold this ground speed, and directs the fishing rod/reel operator to extend/retract the cable to match the target cable length using an integrated cable counter.

All aspects of these sailing flight attempts have been conducted in flight tests at Deland and at the SLF, except the use of the auto-tuning software. The latter is crucial for the aircraft to autonomously refine the target flight conditions, as needed, to achieve a sailing flight mode. Unfortunately, due to delays associated with software development, hardware, and weather, the team was unable to attempt this flight test during the Phase II effort. With internal funding from ERAU, the team expects to be conducting this style of flight test at the SLF during the 2018-2019 academic year.

6.0 Conclusions

The major focus of the Phase II effort described herein was to develop and demonstrate an aircraft capable of autonomously sailing (i.e., to cruise without propulsion or external assistance), and thereby prove that the dual-aircraft platform (DAP) atmospheric satellite concept is potentially viable. This sailing mode of flight was identified as the #1 enabling technology required for the DAP concept in the Phase I effort. No scientific demonstration of this technology has ever been done to our knowledge.

Great strides were made towards development of the enabling technology. A specialized prototype aircraft was developed including a novel cable release mechanism, novel "lateron" control surfaces, and a highly-accurate onboard wind measurement system. All of these devices were developed in house and validated in flight testing. A specialized flight simulator was constructed and utilized to develop the autonomous flight controller required onboard the aircraft, as support training of pilots for flying aircraft while tethered to a ground vehicle. Software has been developed to provide look-up tables that give the flight condition targets (i.e., 3-D position relative to ground vehicle), speed, orientation, and cable length, based on current wind speed and direction. These tables have been successfully validated in flight simulation and used onboard the aircraft. The aerodynamics of this aircraft were characterized with high fidelity analysis, as needed to produce accurate target sailing flight conditions. The aerodynamics of the cable was also accurately characterized using a novel wind tunnel measurement technique. Finally, novel auto-tuning software has been developed to refine the sailing flight condition targets based on an optimization technique involving doublet maneuvers.

Although a real-world demonstration of the sailing mode of flight was not achieved during the Phase II effort, the concept has been further validated using detailed flight simulations and in precursor real-world flight tests. Virtual flights using the auto-tuning software indicate that the prototype aircraft should be able to reach and hold sailing conditions despite moderate levels of turbulence provided there is sufficient mean wind available. Hundreds of flight tests using primarily a dead runway at Deland Municipal Airport, and the long runway at Space Florida's Shuttle Landing Facility, resulted in successful demonstration of the closed-loop autonomous formation flight capability.

Future work should include flight testing (and refinement) of the auto-tune software to refine the aircraft orientation targets and achieve and hold the sailing mode of flight. It is also suggested that higher fidelity onboard avionics may be necessary to facilitate sailing by reducing sensor errors. Although the DAP flight simulator, developed within the Matlab-Simulink framework, includes detailed treatment of aircraft/cable aerodynamics, cable dynamics, experimentally-derived propeller-motor thrust curves, and realistic air turbulence, realistic emulation of various sensor errors, more realistic actuator responsiveness, and hardware-in-the-loop testing is highly desirable to improve the fidelity of flight simulation evaluations of the onboard flight software.

.

Acknowledgements

The DAP team gratefully acknowledge the NASA Innovative Advanced Concepts (NIAC) program, led by Mr. Jason Derleth, for providing the Phase II funding to develop, build, and flight test the Dual Aircraft Platform prototype system. We would also like to thank ERAU for providing extensive use of a pick-up truck to support flight testing, the Vega supercomputer for aerodynamics analysis, and supplementary financial support.

The PI would like to thank all the undergraduate and graduate students that supported this effort. A 2nd year team photo taken with a test aircraft on the ERAU Daytona Beach campus in front of the Wright Flyer is shown below.

References

[1] W. Engblom, "Development of an Atmospheric Satellite Concept Based On Sailing," 52nd Aerospace Sciences Meeting, AIAA SciTech Conference, AIAA 2014-1111.

[2] W. Engblom, W., Dual-Aircraft Atmospheric Platform, U.S. Patent Application No. 13/414,451, March 17, 2012.

[3] W. Engblom and R. Decker, "Virtual Flight Demonstration of the Stratospheric Dual-Aircrafat Platform," 34th AIAA Applied Aerodynamics Conference, AIAA 2016-3877.

[4] W. Engblom, R. Decker, H. Moncayo, W. Barott, E. Sanchez and A. Giovagnoli, "Virtual Flight Demonstration of the Stratospheric Dual-Aircraft Platform," NIAC Phase I Final Report, 2016.

[5] C. Nshuti, W. Engblom, H. Moncayo and D. Festa, "Modeling, Simulation and Flight Testing to Support Proof of a Stratospheric Dual Aircraft Platform Concept," AIAA SciTech Conference, AIAA 2018-1492.

[6] G. Campa, "Airlib," MATLAB Central, 18 June 2009. [Online]. Available: http://www.mathworks.com/matlabcentral/fileexchange/3019-airlib.

[7] N. Coulter, H. Moncayo, and W. Engblom, "Development and Demonstration of a Flight Simulator for the Dual-Aircraft Platform Concept", 2018 Modeling and Simulation Technologies Conference, AIAA AVIATION Forum, AIAA 2018-3886.

[8] J. Willems, W. Engblom, "Verification, Validation, and Application of Shear Stress Transport Transitional Model to a R/C Aircraft," in AIAA SciTech Conference, AIAA 2018-2059.

[9] G. Campa, M. R. Napolitano, B. Seanor and M. G. Perhinschi, "Design of Control Laws for Maneuvered Formation Flight," in American Control Conference, 2004.

[10] Nolan Coulter, Hever Moncayo, and William A. Engblom. "Development and Demonstration of a Flight Simulator for the Dual-Aircraft Platform Concept", 2018 Modeling and Simulation Technologies Conference, AIAA AVIATION Forum, (AIAA 2018-3886)